16th CONGRESS Lung ON CANCER

BARCELONA 27 / 28 NOVEMBER 2025

GECP lung cancer research

Radiomics in lung cancer applied to diagnosis and prediction

María Jesús Ledesma Carbayo

Universidad Politécnica de Madrid

ciber | BBN

POLITÉCNICA

CONFLICTO DE INTERESES

En cumplimiento con el Código de Buenas Prácticas de la Industria Farmacéutica (Farmaindustria), se informa que toda la información compartida durante esta reunión científico-profesional es estrictamente confidencial, privilegiada y destinada únicamente al destinatario previsto. Queda expresamente prohibida la difusión, directa o indirecta, a través de redes sociales, canales de comunicación o medios externos, así como cualquier uso no autorizado, incluida la divulgación o distribución del contenido.

La información presentada no debe ser utilizada con fines promocionales, ni constituye asesoramiento médico o actividades promocionales. Además, contiene propuestas preliminares, planes, estrategias y opiniones que no representan posiciones finales ni garantías de desempeño futuro. En caso excepcional de que desee compartir algún contenido, deberá contar con la autorización previa, expresa y por escrito de **GECP.**

AI paradigm change

Clinical Biomarkers

Symptoms

Molecular and histological Biomarkers

Image Based Biomarkers

AI and Image processing

A new way to study disease

New biomarker discovery for patient care

AI paradigm change

Risk Identification

Comorbidities assessment

Therapy response prediction

Prognosis prediction

Image Health Care Analytics

Introduction to radiomics

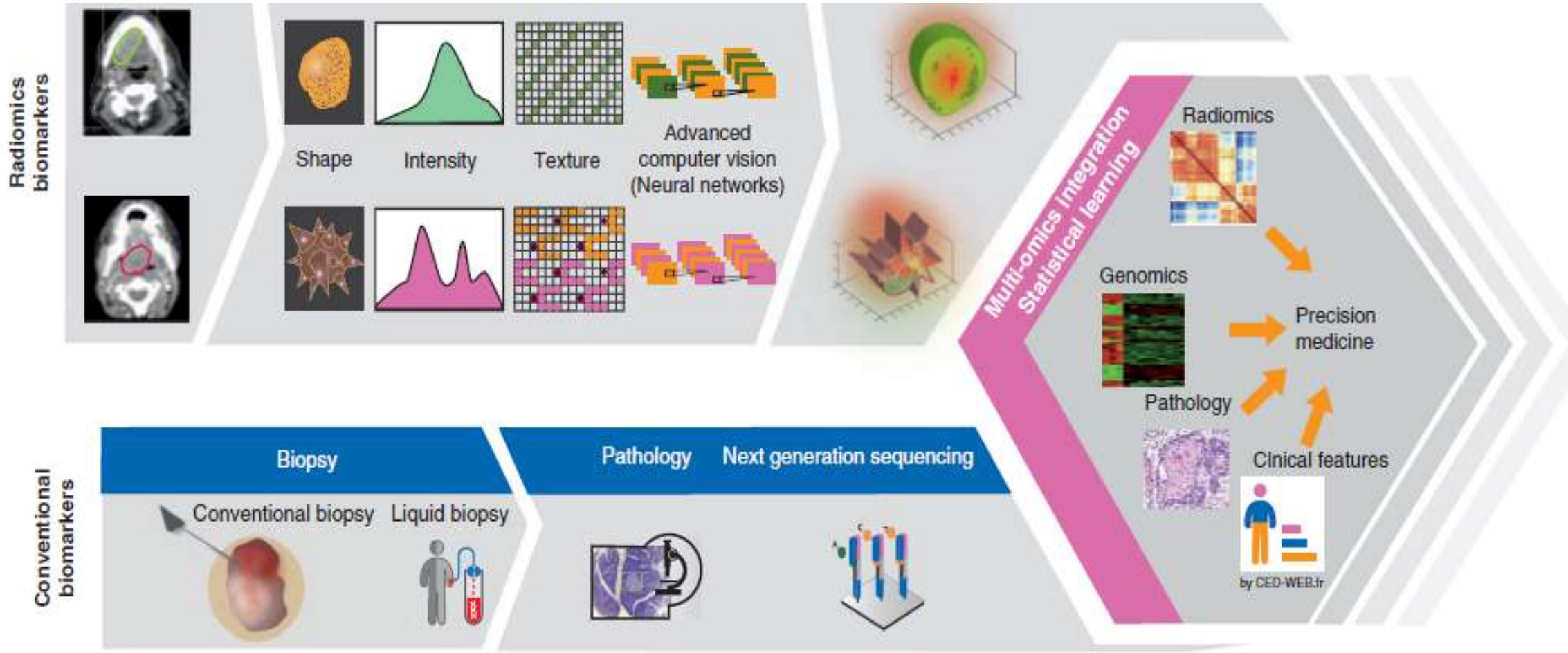

Promises and challenges for the implementation of computational medical imaging (radiomics) in Oncology. Limkin et al Annals of Oncology 2017

Phases of radiomics analysis

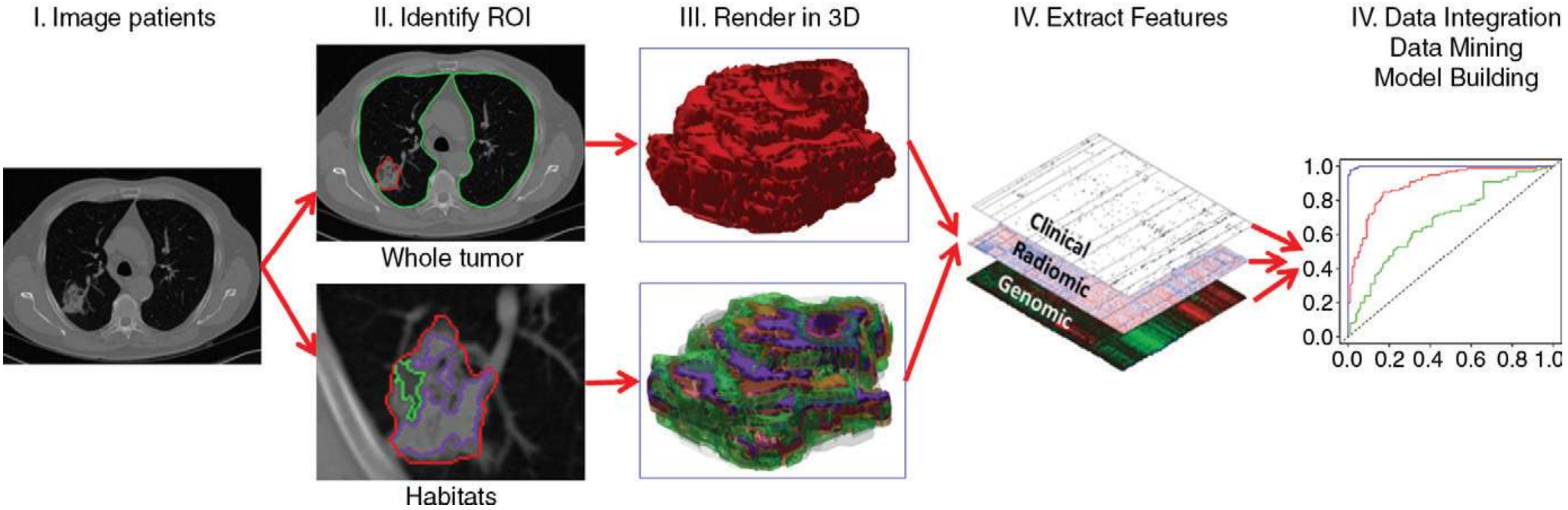

Radiomics: Images Are More than Pictures, They Are Data, Gillies et al. Radiology 2016

Deep-Learning

- Most machine learning algorithms are shallow architectures, but our brain is a deep architecture -

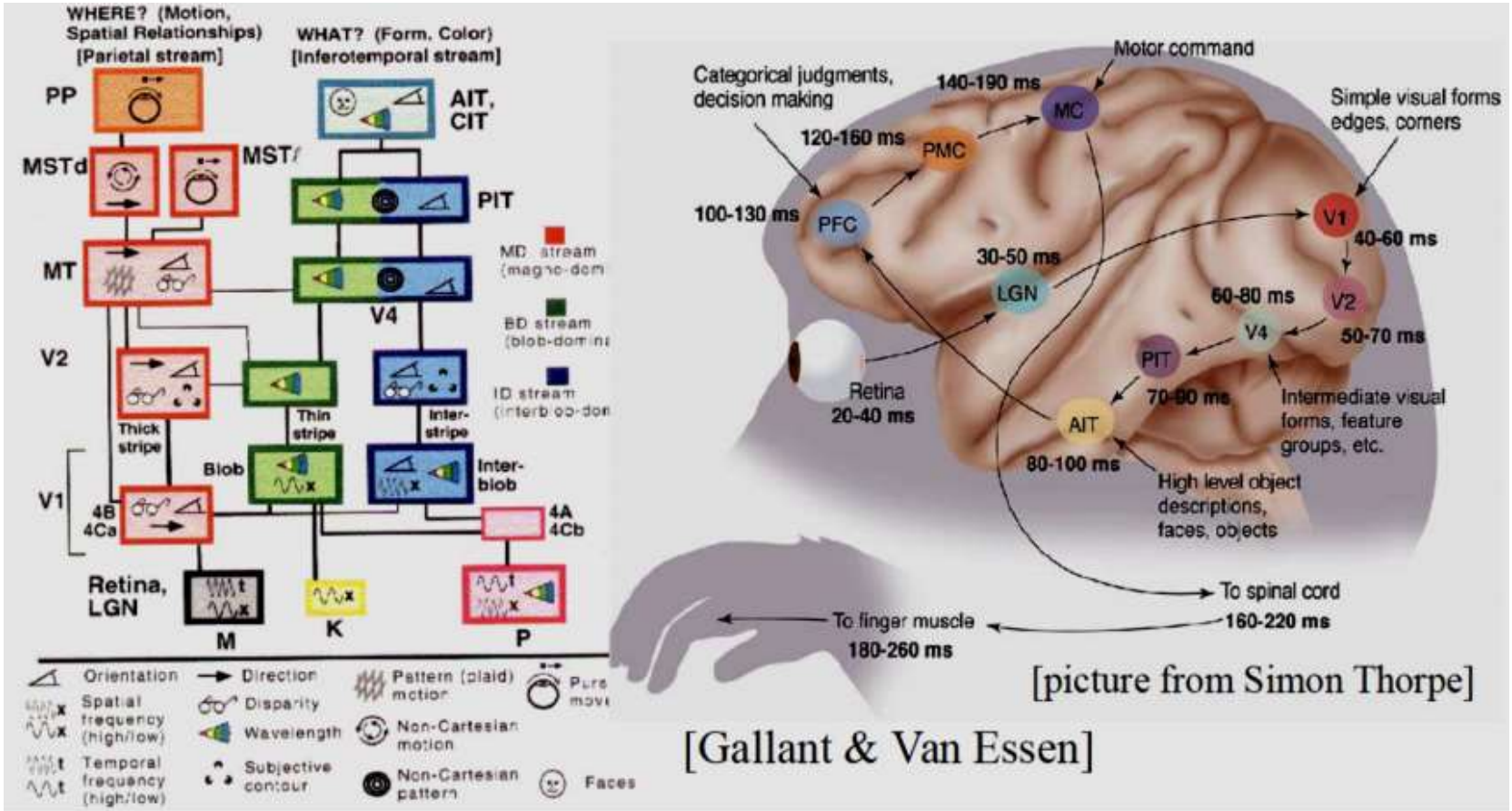

Deep-Learning

- Deep learning assumes it is possible to “learn” a hierarchy of descriptors (features) with increasing abstraction, i.e., layers are trainable feature transforms.
- In image recognition: Pixel → Edge → Texton → Motif → Part → Object.

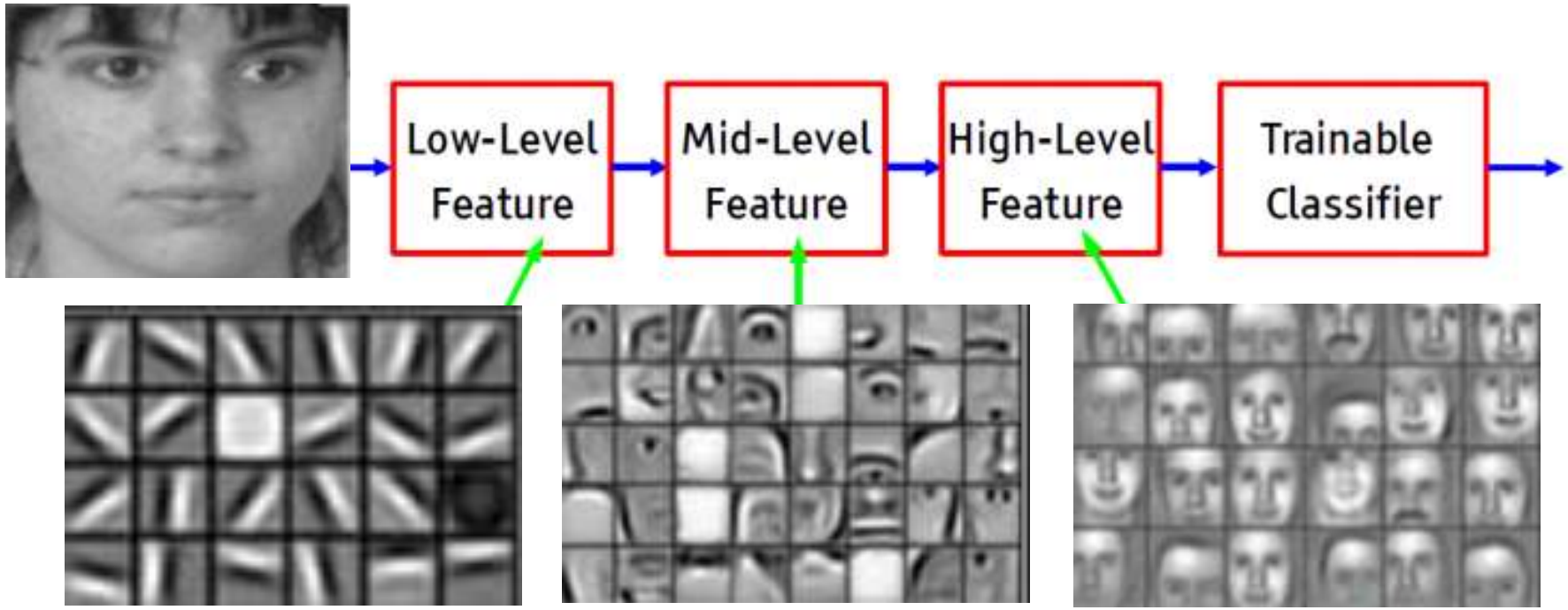

Convolunional Neural Networks

- Convolutional nets were inspired by the visual system's structure.
- CNN are composed by three principal blocks: Convolutional layers / Pooling layers /Fully connected layers

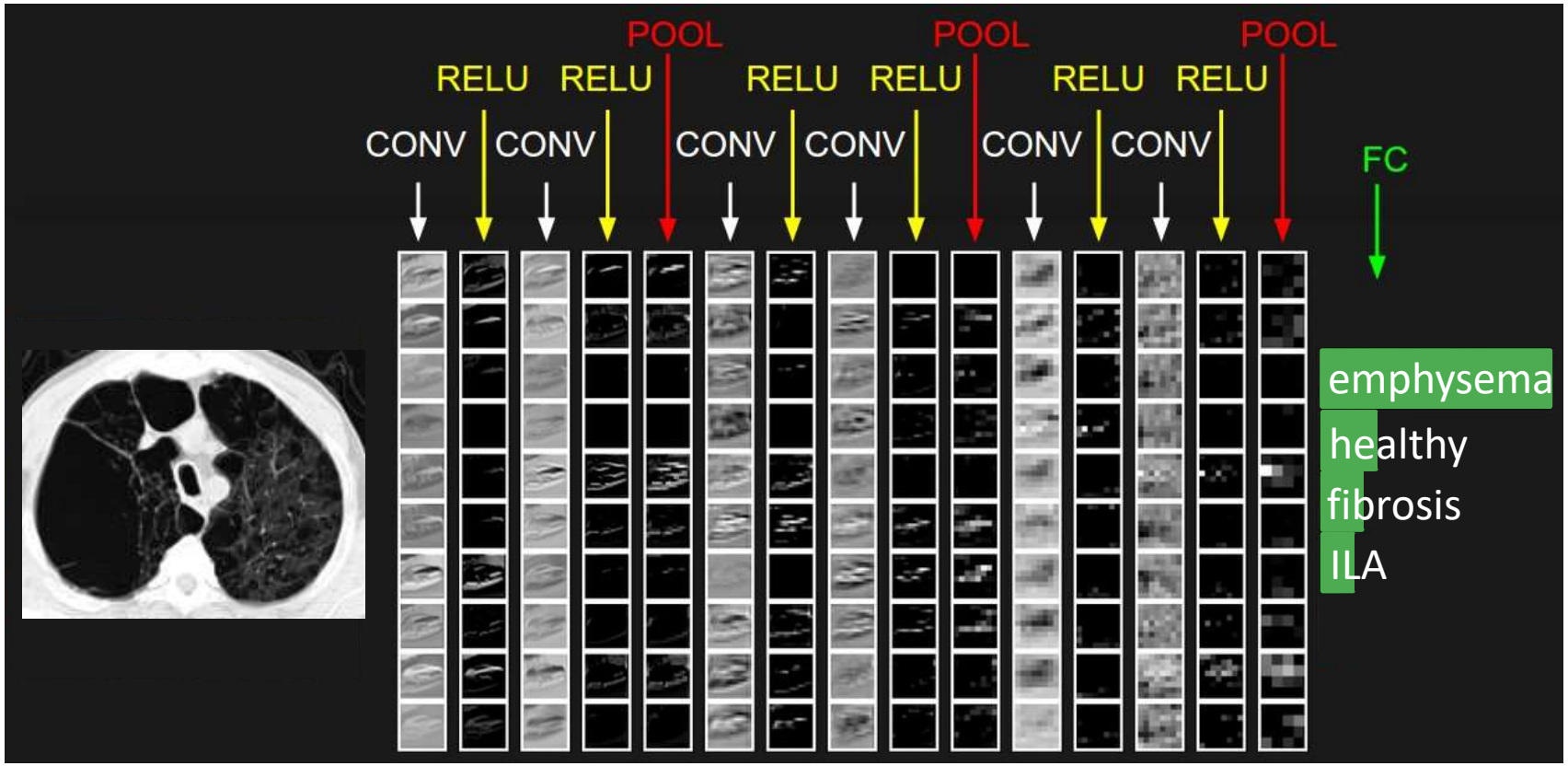

Radiomics and deep learning in Cancer

- **Tumor heterogeneity-** tumor environment may present many subclones with different biological substrate

- Can we quantify or characterize macroscopically that substrate??

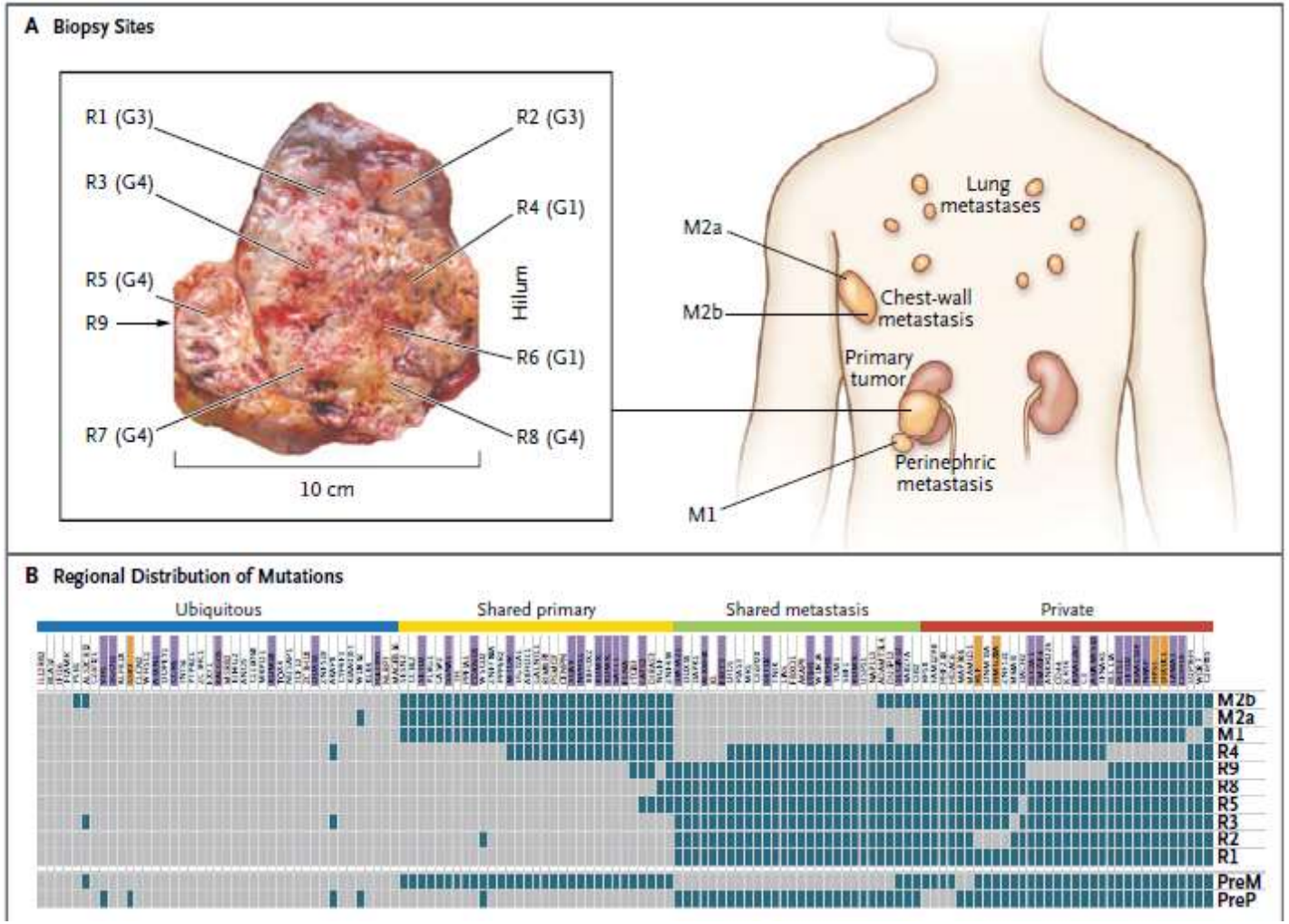

Intratumor Heterogeneity and Branched Evolution Revealed by Multiregion Sequencing, Gerlinger et al. New England 2012

Radiomics and deep learning in Cancer

- **Prognosis and phenotyping**

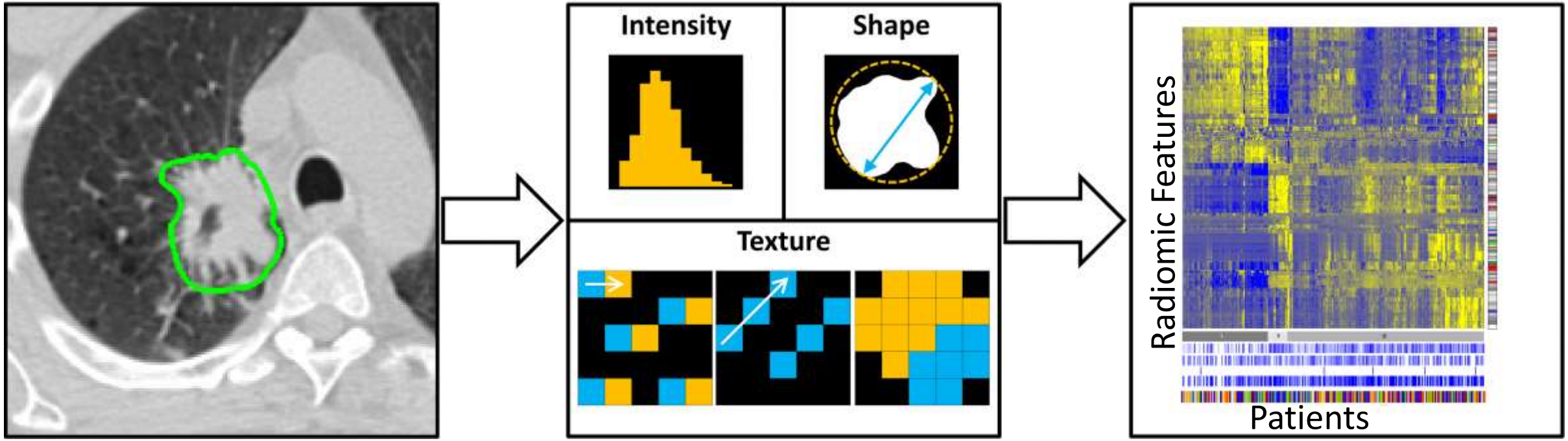

  - 440 radiomic features – Survival prediction signature with 4 features, total energy, shape compactness, LG and Wavelet gray level nonuniformity
  - Model selection/ Training with one cohort 422 NSCLC

Aerts H. et al. Nature Communications 2014

Radiomics and deep learning in Cancer

- **Prognosis and phenotyping**

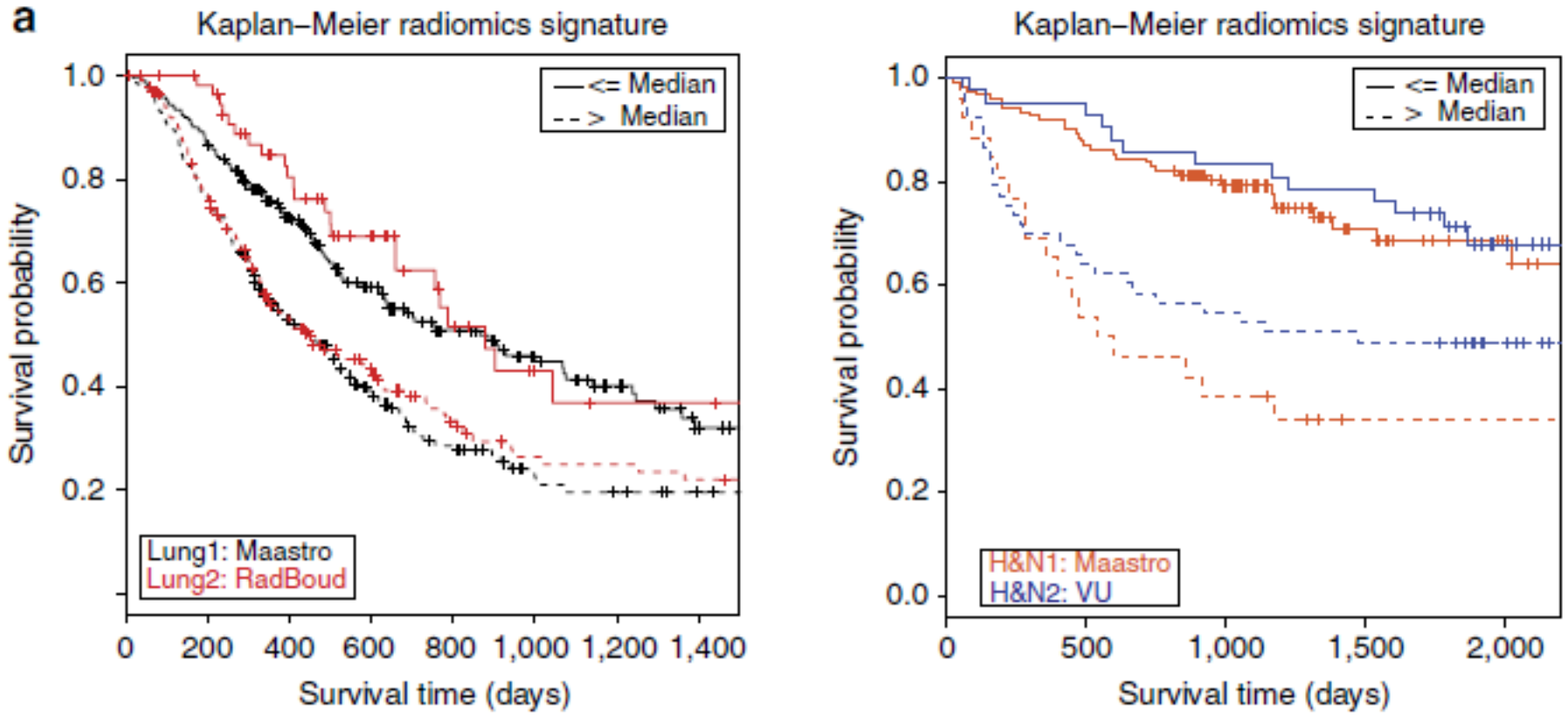

  - Validation with 4 independent cohorts: 2 NSCLC, 2 HNC – total 1019 patients
  - Gen-expresions to radiomics relationships found

Aerts H. et al. Nature Communications 2014

Radiomics in Lung Cancer Diagnosis

- **Benign vs Malignant**
  - Radiomics + Deep learning strategy
  - Data from the Lung Image Database Consortium LIDC data: 1018 patients, 4 radiologist reading, 157 with diagnostic confirmation from biopsy.
  - Training: 80% of 1065 nodules
  - Testing : 20% of 1065 nodules independent patients
  - Model: Radiomics + Random Forest and two CNNs tested
  - Comparison with a regression model of the cross sectional area.

Highly accurate model for prediction of lung nodule malignancy with CT scans. Jason L. Causey at al. Scientific reports 2018

Radiomics in Lung Cancer Diagnosis

- **Classification of lung tumors / Benign vs Malignant**

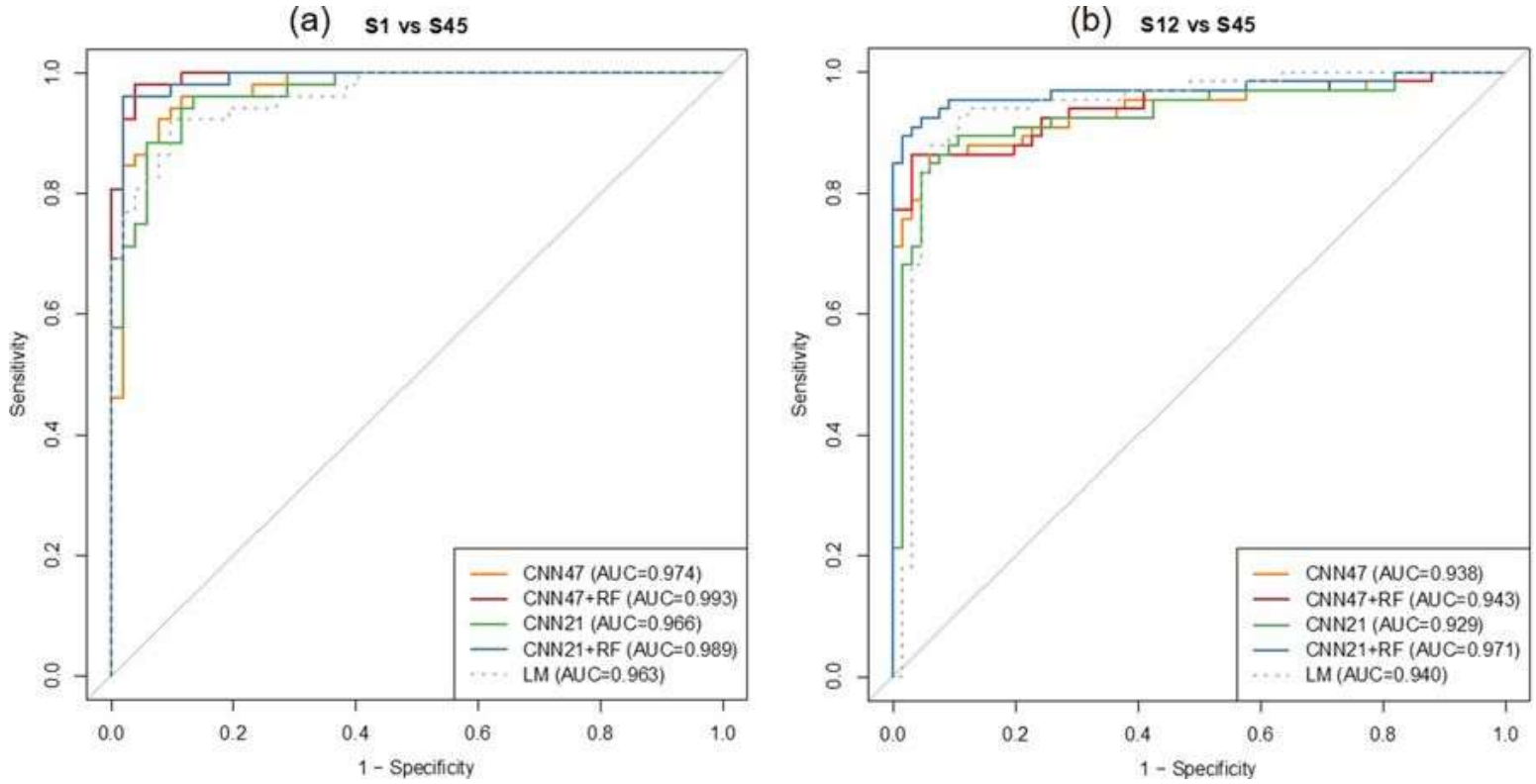

Classification accuracy of benign S1, or S12 vs malignant S45- 0.99 and 0.94 resp.

Highly accurate model for prediction of lung nodule malignancy with CT scans. Jason L. Causey at al. Scientific reports 2018

Radiomics in Lung Cancer Diagnosis

nature medicine

Letter | Published: 20 May 2019

End-to-end lung cancer screening with three-dimensional deep learning on low-dose chest computed tomography

Diego Ardila, Atilla P. Kiraly, Sujeeth Bharadwaj, Bokyung Choi, Joshua J. Reicher, Lily Peng, Daniel Tse ✉, Mozziyar Etemadi, Wenxing Ye, Greg Corrado, David P. Naidich & Shravya Shetty

Nature Medicine **25**, 954–961 (2019) | Cite this article

Two Screening cohorts

AUC 94.4 %

Radiomics in Lung Cancer Diagnosis

- **Lung cancer risk and nodule classification**

Journal of Clinical Oncology
An American Society of Clinical Oncology Journal

CURRENT

OPEN ACCESS | ORIGINAL REPORTS | January 12, 2023

Sybil: A Validated Deep Learning Model to Predict Future Lung Cancer Risk From a Single Low-Dose Chest Computed Tomography

Authors: Peter G. Mikhael, BSc, Jeremy Wohlwend, ME, Adam Yala, PhD, Ludvig Karstens, MSc, Justin Xiang, ME, Angelo [illegible], Patrick P. Bourgouin, MD, ... SHOW ALL ..., and Regina Barzilay, PhD AUTHORS INFO & AFFILIATIONS

J Clin Oncol 41, 2191-2200(2023) • Volume 41, Number 12 • DOI: 10.1200/JCO.22.01345

AUC lung cancer prediction at 1 year of 0.92 (95% CI, 0.88 to 0.95) on NLST, 0.86 (95% CI, 0.82 to 0.90) on MGH, and 0.94 (95% CI, 0.91 to 1.00) on CGMH. Concordance indices over 6 years were 0.75 (95% CI, 0.72 to 0.78), 0.81 (95% CI, 0.77 to 0.85), and 0.80 (95% CI, 0.75 to 0.86) for NLST, MGH, and CGMH, respectively.

Cancer Enriched cohort - AUC 0.79 versus 0.60 PanCan model ($P < .01$)
40% reduction false positives at 100% sensitivity.

Radiology

ORIGINAL RESEARCH

External Test of a Deep Learning Algorithm for Pulmonary Nodule Malignancy Risk Stratification Using European Screening Data

Noa Antonissen, MD[1] • Kiran Vaidhya Venkadesh, PhD[1] • Renate Dinnessen, MSc[1] • Ernst Th. Scholten, MD, PhD[1] • Zaigham Saghir, MD, PhD[2,3] • Mario Silva, MD, PhD[4] • Ugo Pastorino, MD[5] • Grigory Sidorenkov, PhD[6,7] • Marjolein A. Heuvelmans, MD, PhD[6,8] • Geertruida H. de Bock, PhD[9] • Firdaus A. A. Mohamed Hoesein, MD, PhD[9] • Pim A. de Jong, MD, PhD[9] • Harry J. M. Groen, MD, PhD[10] • Rozemarijn Vliegenthart, MD, PhD[7] • Hester A. Gietema, MD, PhD[11,12] • Mathias Prokop, MD, PhD[1] • Cornelia Schaefer-Prokop, MD, PhD[1,13] • Colin Jacobs, PhD[1] • for the NELSON-POP consortium[14]

Author affiliations, funding, and conflicts of interest are listed at the end of this article.

[14] NELSON-POP consortium members are listed in Appendix S1.

Radiology 2025; 316(3):e250874 • https://doi.org/10.1148/radiol.250874 • Content codes: CH IN AI

Lung Cancer Screening: Longitudinal deep-learning architecture for nodule malignancy classification

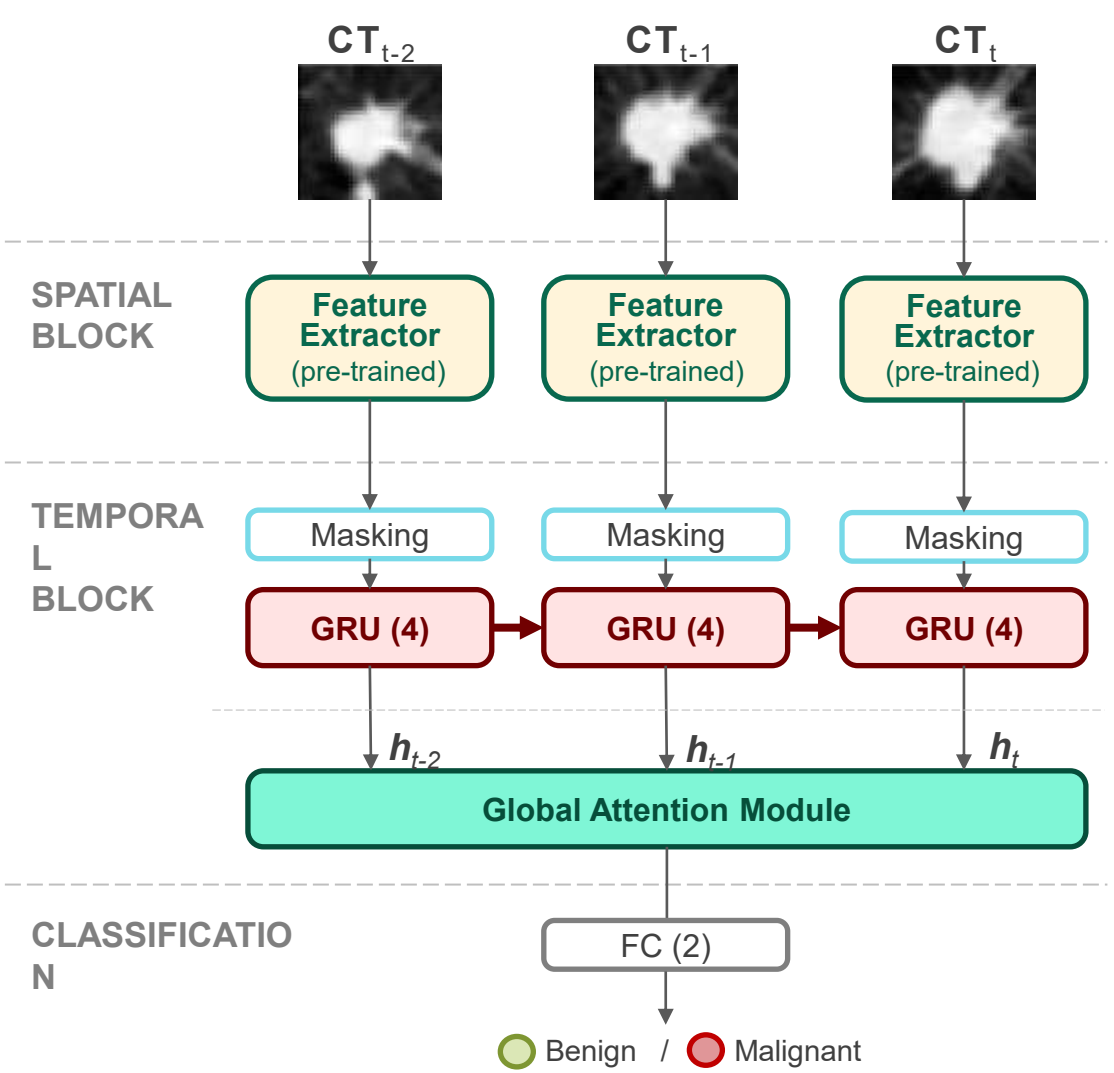

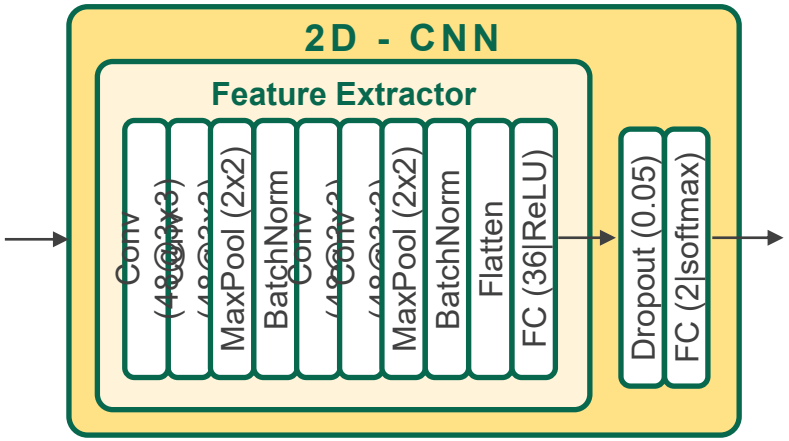

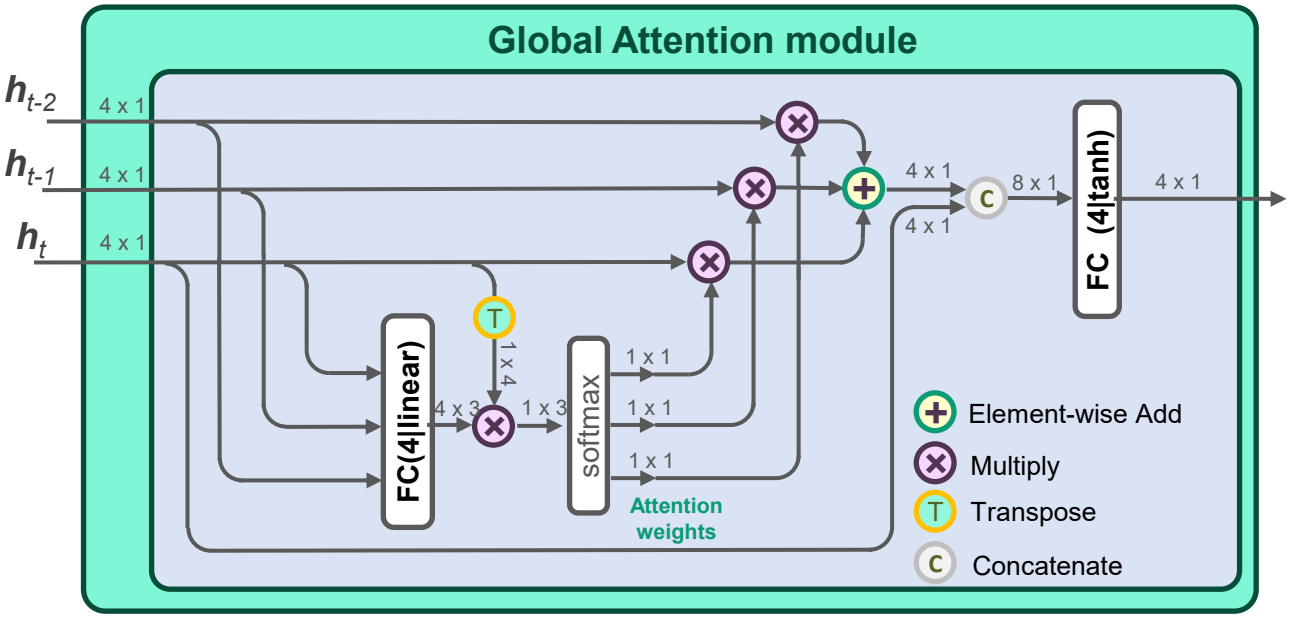

Farina, B., ... & Ledesma-Carbayo, M. J. Spatio-Temporal Deep Learning with Temporal Attention for Indeterminate Lung Nodule Classification. under review by Computers in Biology and Medicine

Lung Cancer Screening: Longitudinal deep-learning architecture for nodule malignancy classification

NLST indeterminate nodules

	Total	Train	Test
Patients	443	333	110
Non-cancer	235	176	59
Cancer	208	157	51
Nodules	703	528	175
Benign	486	365	121
Malignant	217	163	54

Table 2

Comparisons results of models evaluated on the independent test set. For each metric, the 95% confidence interval is shown in brackets. DeLong test was used to compare AUCs

Model	Time instant	N nodules test	AUC [95% CI]	ACC [95% CI]	SENS [95% CI]	SPEC [95% CI]	PREC [95% CI]	bACC [95% CI]	*p*-value
globAttCRNN (GRU)	T0 - T1 - T2	175	0.954 [0.922,0.983]	0.897 [0.851,0.937]	0.870 [0.774,0.959]	0.909 [0.856,0.957]	0.810 [0.707,0.905]	0.890 [0.838,0.941]	–
globAttCRNN (LSTM)	T0 - T1 - T2	175	0.924 [0.873, 0.971]	0.869 [0.817, 0.914]	0.870 [0.783, 0.959]	0.868 [0.805, 0.924]	0.746 [0.641, 0.844]	0.869 [0.816, 0.922]	0.0145
CNN-DLSTM	T0 - T1 - T2	175	0.927 [0.878, 0.969]	0.829 [0.771, 0.886]	0.889 [0.800, 0.966]	0.802 [0.730, 0.870]	0.667 [0.561, 0.771]	0.845 [0.790, 0.900]	0.0296
Volume-doubling time LR	Tlast-Tprevioustolast	175	0.849 [0.772, 0.916]	0.823 [0.766, 0.880]	0.444 [0.316, 0.582]	0.992 [0.974, 1.000]	0.960 [0.870, 0.000]	0.718 [0.653, 0.789]	0.0042
Largest In-plane Diameter LR	Tlast	175	0.918 [0.874, 0.958]	0.714 [0.646, 0.777]	0.130 [0.049, 0.220]	0.975 [0.946, 1.000]	0.700 [0.385, 1.000]	0.552 [0.510, 0.599]	0.0496
CNN	Tlast	175	0.916 [0.861,0.964]	0.846 [0.789,0.897]	0.796 [0.685,0.9]	0.868 [0.805,0.924]	0.729 [0.614,0.837]	0.832 [0.768,0.893]	0.0064

Farina, B., ... & Ledesma-Carbayo, M. J. Spatio-Temporal Deep Learning with Temporal Attention for Indeterminate Lung Nodule Classification. *Comput. Biol. Med.*, 196(Pt C):110813. Sep. 2025.

Immunotherapy response prediction

Current methods to predict response imperfect

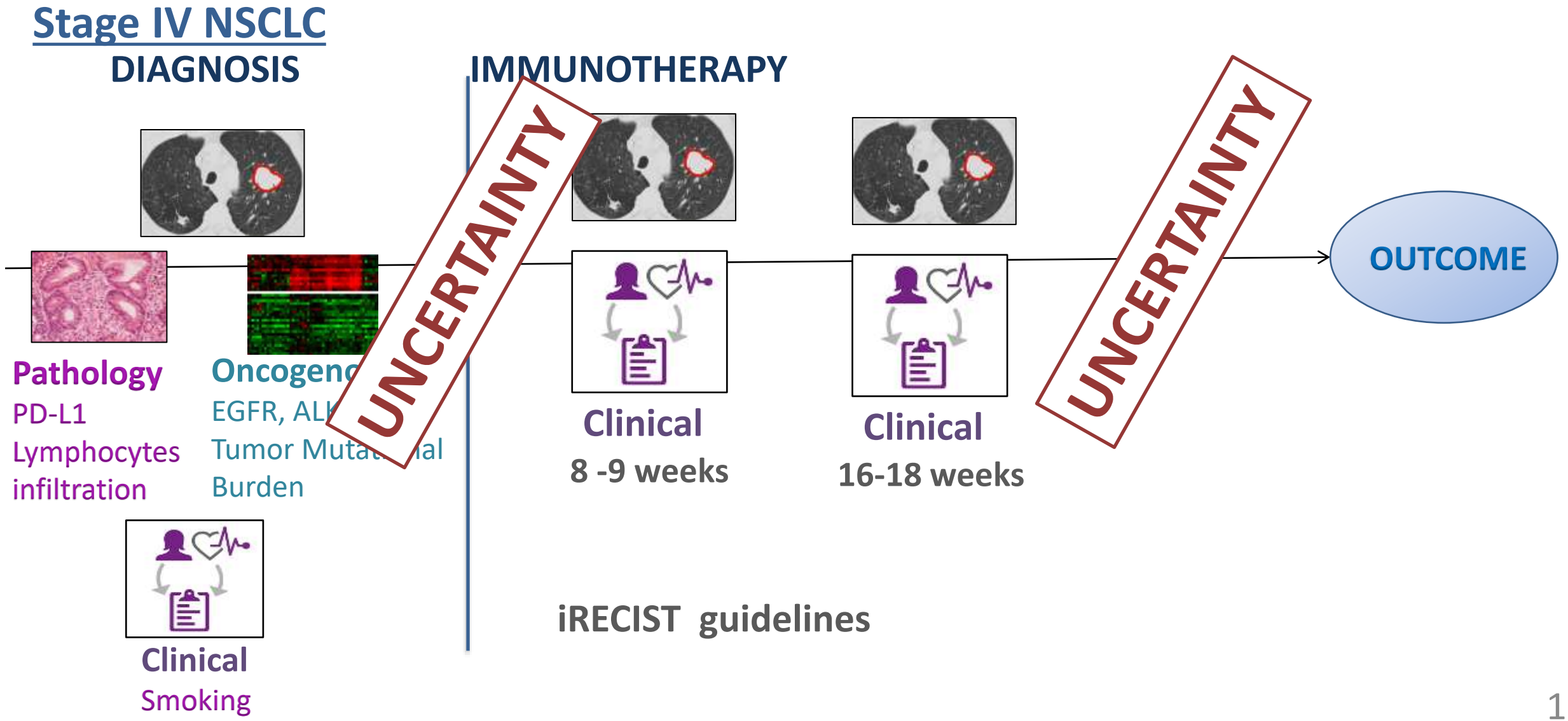

Immunotherapy response prediction

- **Predicting immune related variables**
  - Training - 135 patients (30 LC), genomic data CD8B gene
  - 78 radiomic features, five location variables an on CT variable
  - Separated analysis of the peripheral ring of the tumor
  - CD8 T cell prediction using radiomics
  - Validation, 3 cohorts

A radiomics approach to assess tumour-infiltrating CD8 cells and response to anti-PD-1 or anti-PD-L1 immunotherapy: an imaging biomarker, retrospective multicohort study, Sun et al. Lancet Oncology, 2018

Immunotherapy response prediction

- **Predicting immune related variables**

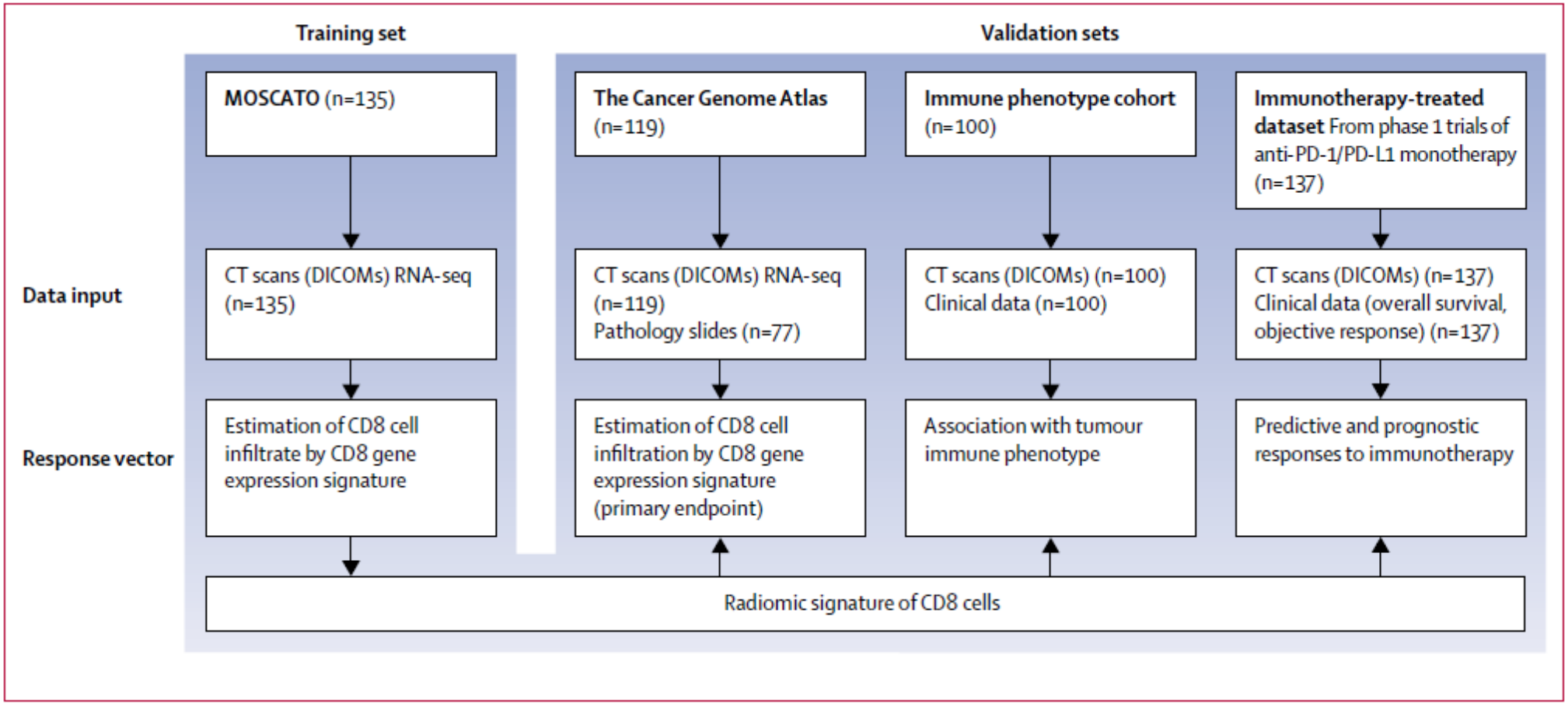

A radiomics approach to assess tumour-infiltrating CD8 cells and response to anti-PD-1 or anti-PD-L1 immunotherapy: an imaging biomarker, retrospective multicohort study, Sun et al. Lancet Oncology, 2018

Immunotherapy response prediction

- **Predicting immune related variables**

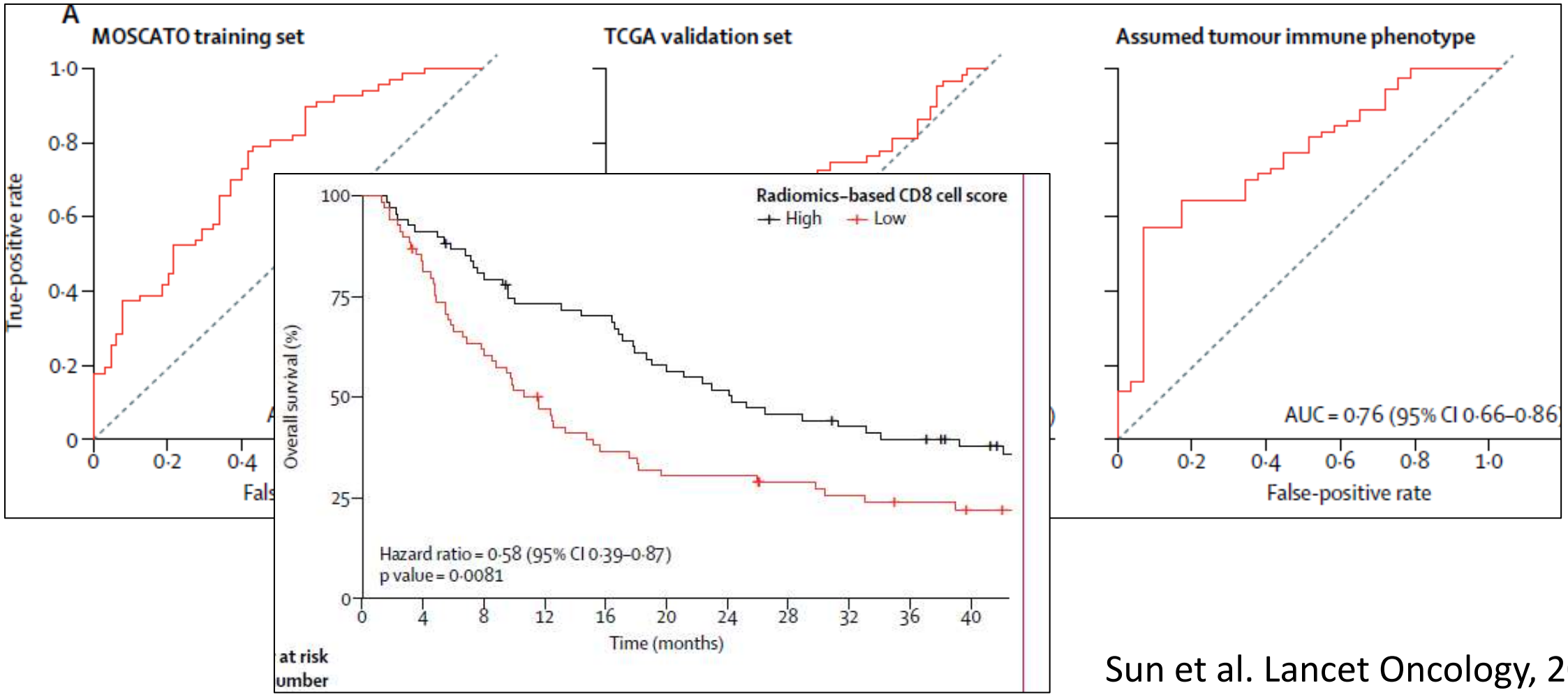

Sun et al. Lancet Oncology, 2018

Immunotherapy response prediction

Article | Open access | Published: 29 August 2022

Multimodal integration of radiology, pathology and genomics for prediction of response to PD-(L)1 blockade in patients with non-small cell lung cancer

Rami S. Vanguri, Jia Luo, Andrew T. Aukerman, Jacklynn V. Egger, Christopher J. Fong, Natally Horvat, Andrew Pagano, Jose de Arimateia Batista Araujo-Filho, Luke Geneslaw, Hira Rizvi, Ramon Sosa, Kevin M. Boehm, Soo-Ryum Yang, Francis M. Bodd, Katia Ventura, Travis J. Hollmann, Michelle S. Ginsberg, Jianjiong Gao, MSK MIND Consortium, Matthew D. Hellmann, Jennifer L. Sauter ✉ & Sohrab P. Shah ✉

Nature Cancer **3**, 1151–1164 (2022) | Cite this article

Immunotherapy response prediction

- **NSCLC**
  - 247 stage IV patients
  - anti-PDL1 immunotherapy
  - 25% responders
  - Multimodal baseline data: radiomics, genomics, and histopathology
  - 256 patients independent validation cohort
  - 0.80 AUC immunotherapy response. Integrated model improves on individual models, including the tumor mutational burden-based model (0.61 AUC), or radiomics only (0.65)

Vanguri et al. 2022

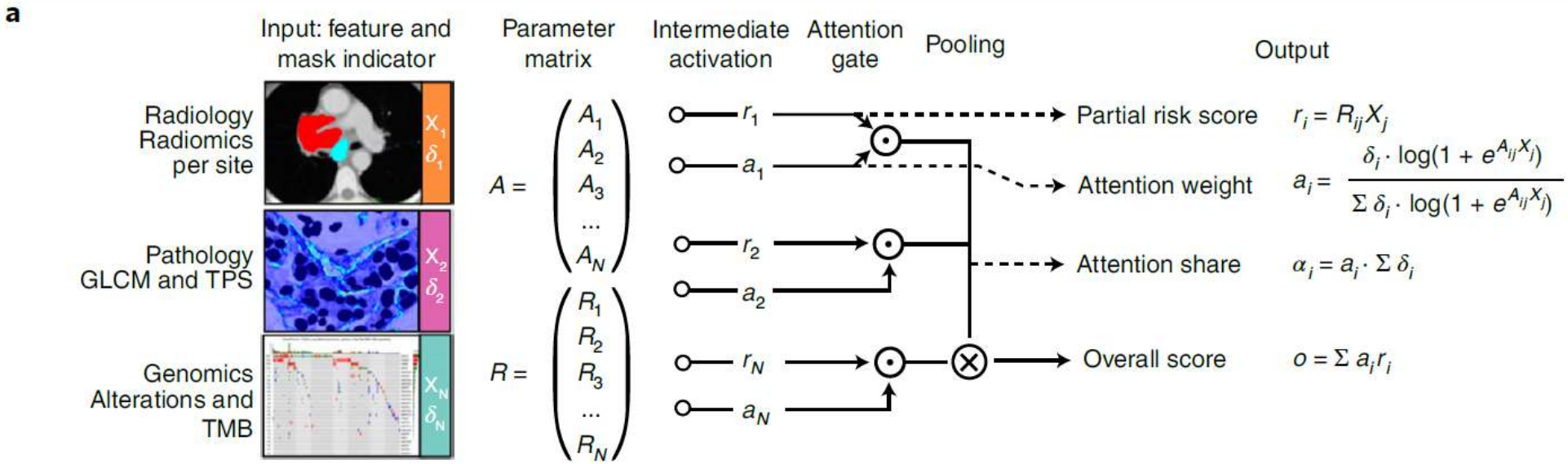

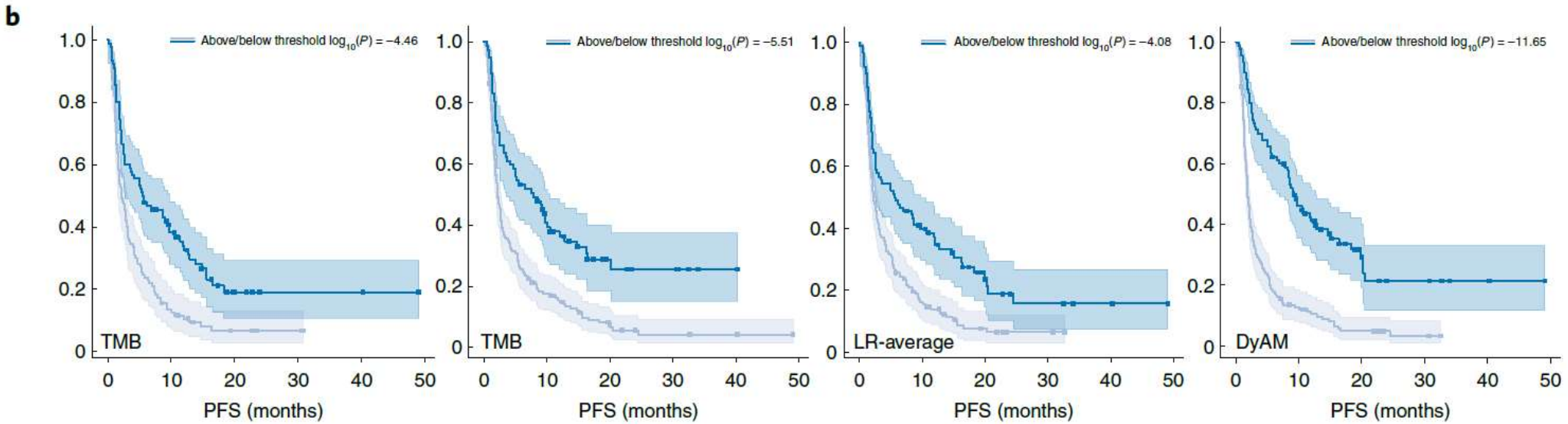

Above threshold																								
At risk	111	14	4	2	0	0	170	28	8	3	2	0	157	23	7	3	0	0	157	18	6	2	0	0
Censored	0	2	6	8	10	10	0	3	9	11	12	14	0	4	10	13	16	16	0	3	5	8	10	10
Events	0	95	101	101	101	101	0	139	153	156	156	156	0	130	140	141	141	141	0	136	146	147	147	147
Below threshold																								
At risk	90	30	6	3	3	0	77	28	9	5	1	0	90	33	10	5	3	0	90	38	11	6	3	0
Censored	0	5	17	20	20	23	0	4	16	19	23	24	0	3	15	17	19	22	0	4	20	22	25	28
Events	0	55	67	67	67	67	0	45	52	53	53	53	0	54	65	68	68	68	0	48	59	62	62	62

Vanguri et al. 2022

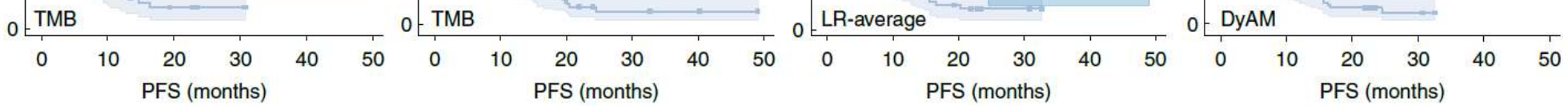

Above threshold																								
At risk	111	14	4	2	0	0	170	28	8	3	2	0	157	23	7	3	0	0	157	18	6	2	0	0
Censored	0	2	6	8	10	10	0	3	9	11	12	14	0	4	10	13	16	16	0	3	5	8	10	10
Events	0	95	101	101	101	101	0	139	153	156	156	156	0	130	140	141	141	141	0	136	146	147	147	147
Below threshold																								
At risk	90	30	6	3	3	0	77	28	9	5	1	0	90	33	10	5	3	0	90	38	11	6	3	0
Censored	0	5	17	20	20	23	0	4	16	19	23	24	0	3	15	17	19	22	0	4	20	22	25	28
Events	0	55	67	67	67	67	0	45	52	53	53	53	0	54	65	68	68	68	0	48	59	62	62	62

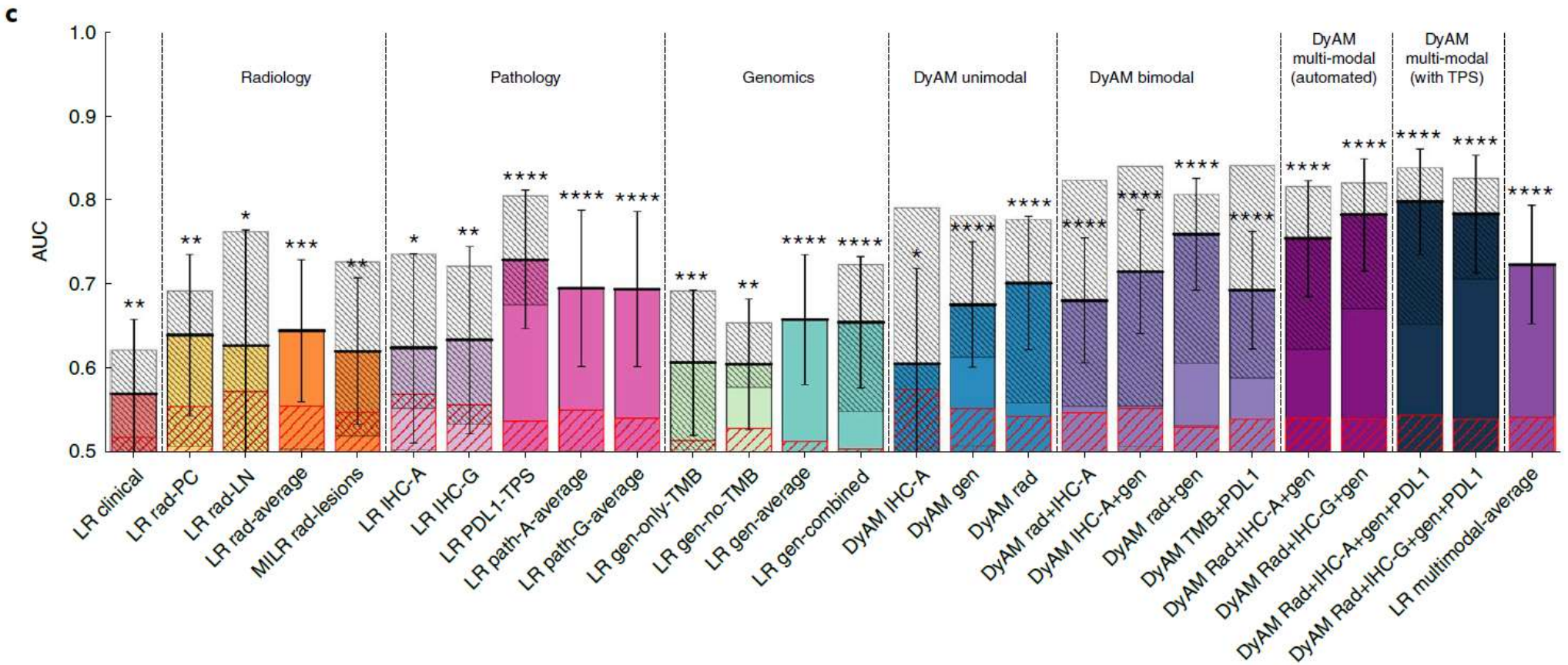

Vanguri et al. 2022

Spatio-temporal Immunotherapy response prediction

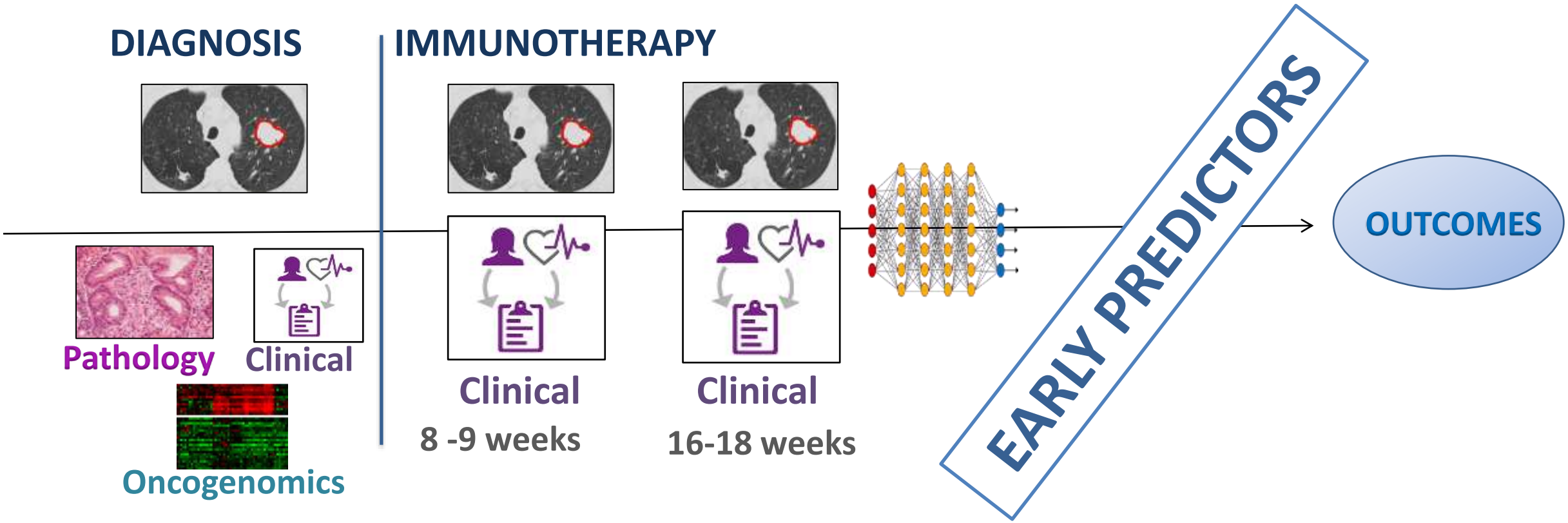

- **Prediction of response directly from CT images and their integration with clinical data and blood tests at the start of treatment.**

Farina et al. J Trans Med 2023

Spatio-temporal Immunotherapy response prediction

1. **Characterization dataset** for feature extraction.
2. **Immunotherapy dataset** for implementation of predictive models

Characterization dataset	N patients	N nodules/ N images
LIDC	689	1447 / 689
ISBI	30	52 / 30
FJD-CUN	14	29 / 14
Total	733	1528 / 733

Immunotherapy dataset	N patients/ N images	Removed patients *	Total
CUN	76 / 202	5	75 / 198
FJD	110 / 312	14	96 / 282
Total	186 / 514	15	**171** / 480 **

* Patients without progression with a LFU < 6 months

OUTPUT	**N nodules**
Benign	1024
Malignant	504

OUTPUT	**N patients**
No responders	94
Responders	77

Spatio-temporal Immunotherapy response prediction

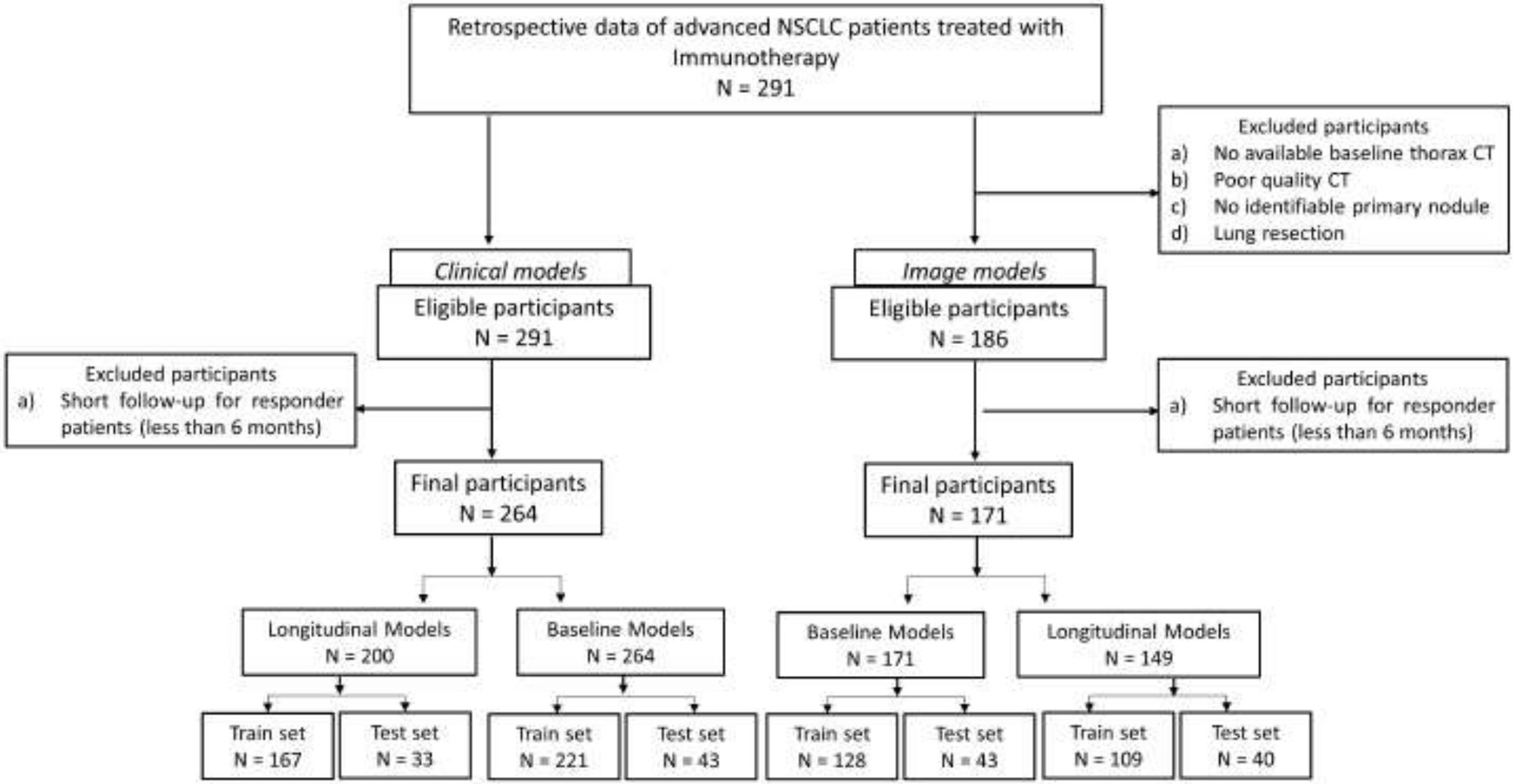

Farina et al 2023 J Transl Med

Spatio-temporal Immunotherapy response prediction

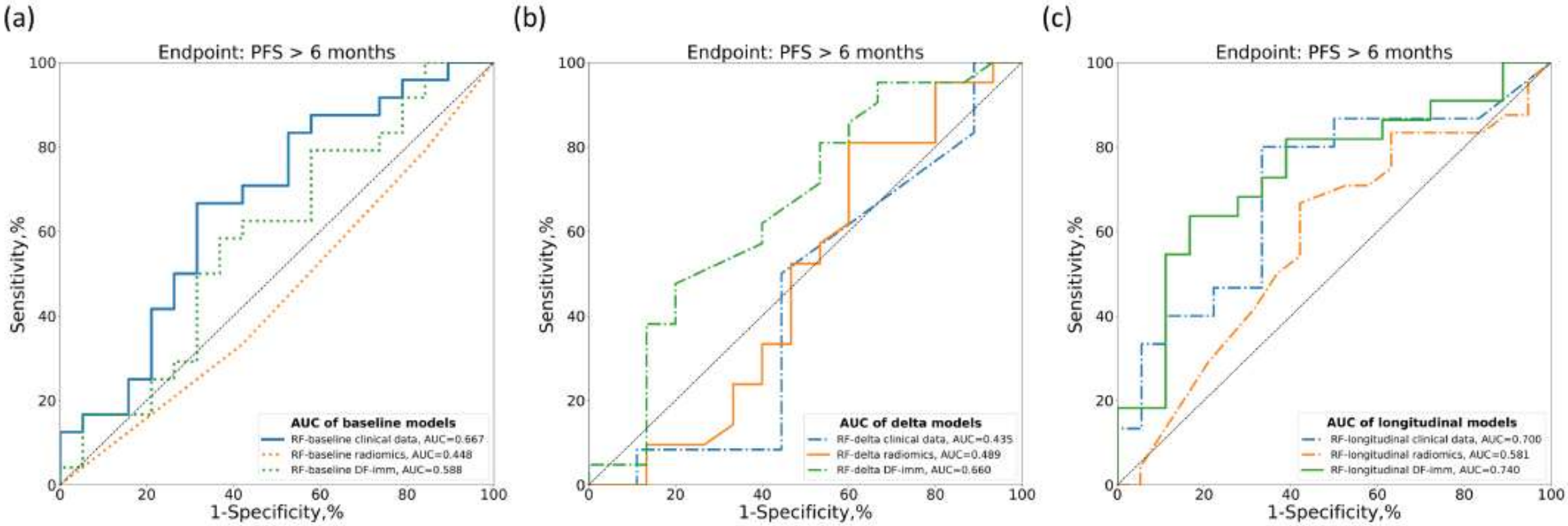

Figure 2. Comparisons of the ROC curves for endpoint PFS6 prediction of response of the baseline (a), delta (b), and longitudinal RF models (c) based on clinical, radiomics, or deep-radiomics data.

Farina et al. J Trans Med 2023

Spatio-temporal Immunotherapy response prediction

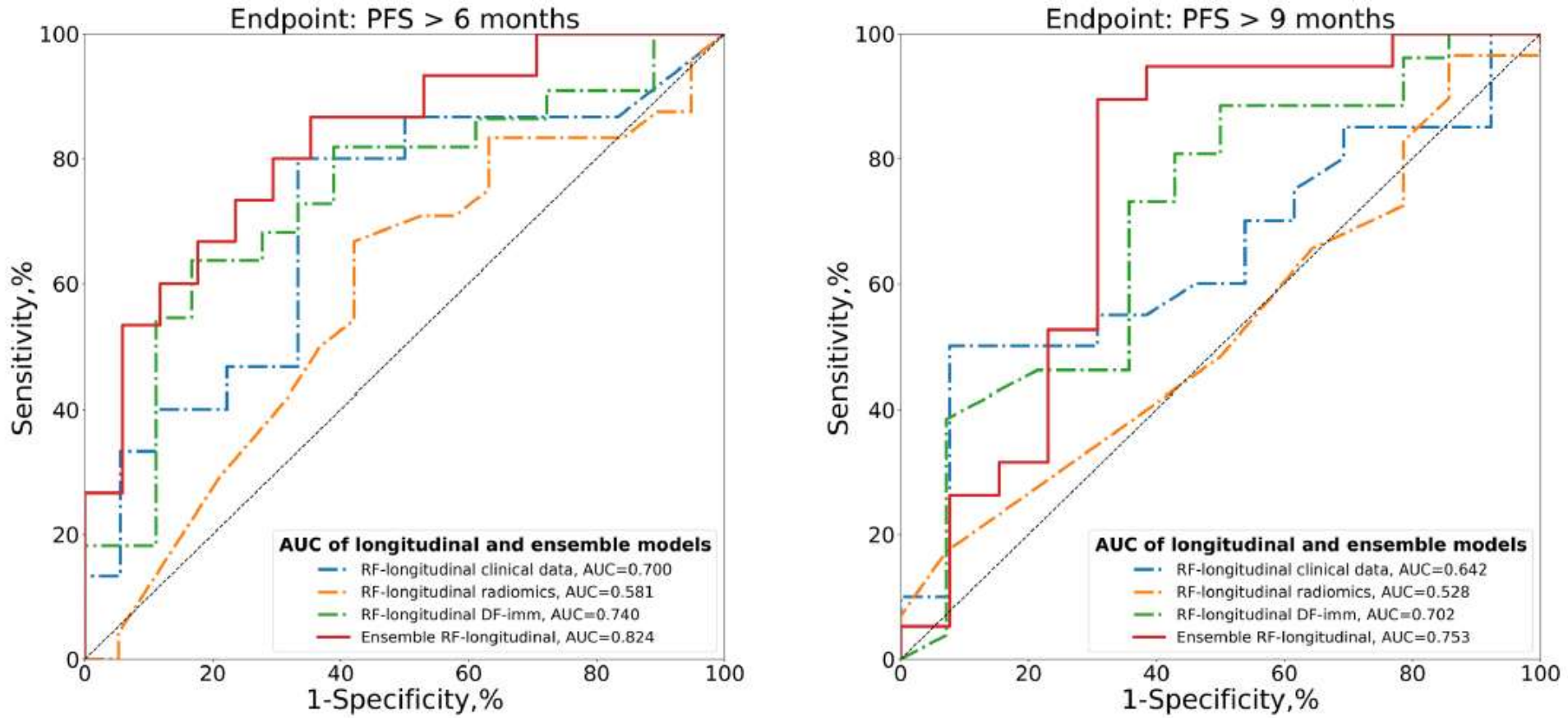

Figure 4. Comparisons of ROC curves of longitudinal and ensemble RF models with clinical and radiomics data. (a) ROC curves for PFS6: PFS > 6 months. (b) ROC curve for PFS9: PFS > 9 months.

Farina et al. J Trans Med 2023

Spatio-tempora Immunotherapy response prediction

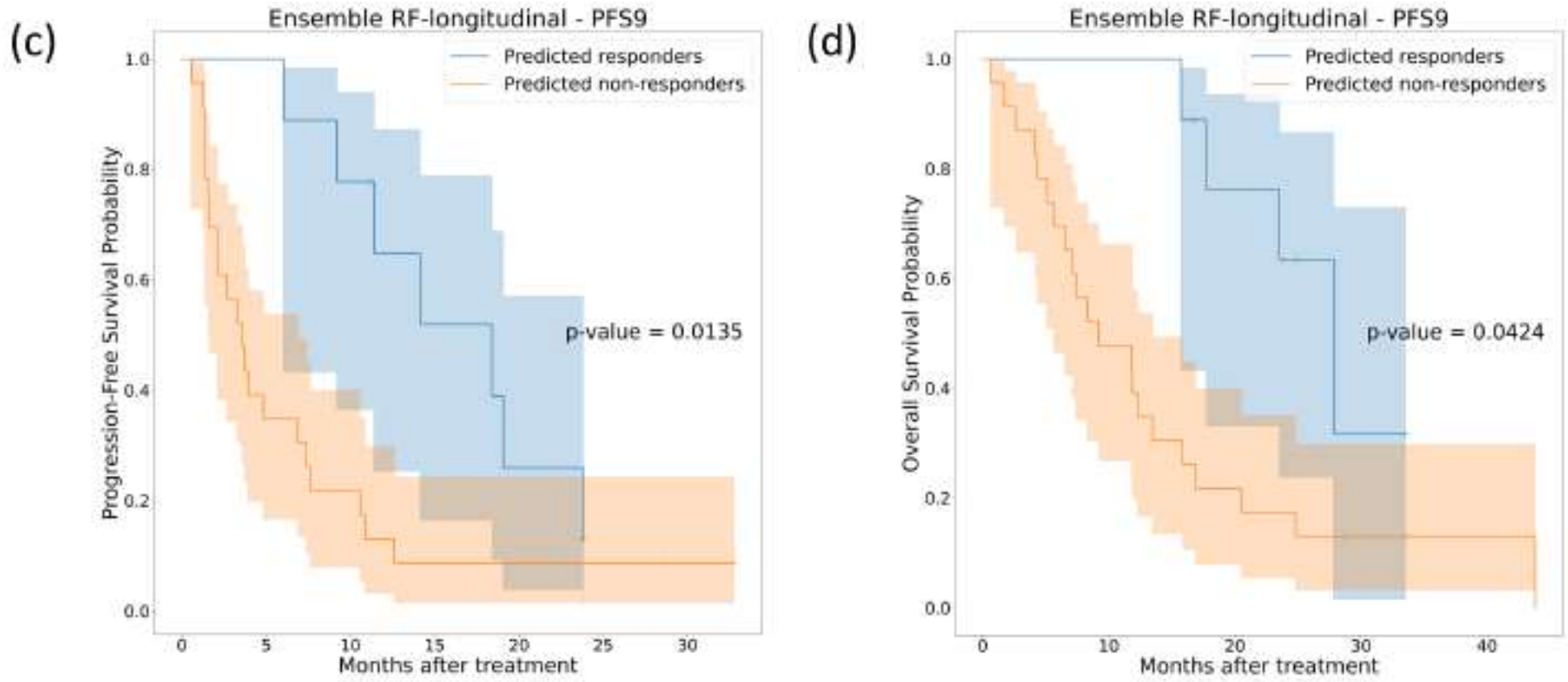

Figure 5. Kaplan-Meier survival curves on the independent test cohort for ensemble RF models trained for endpoint PFS6 (first row) and PFS9 (second row). (a) and (c) represent the PFS Kaplan-Meier curves, while (b) and (d) represent the OS Kaplan-Meier curves.

Farina et al. 2023 J Transl Med

Spatio-temporal Immunotherapy response prediction

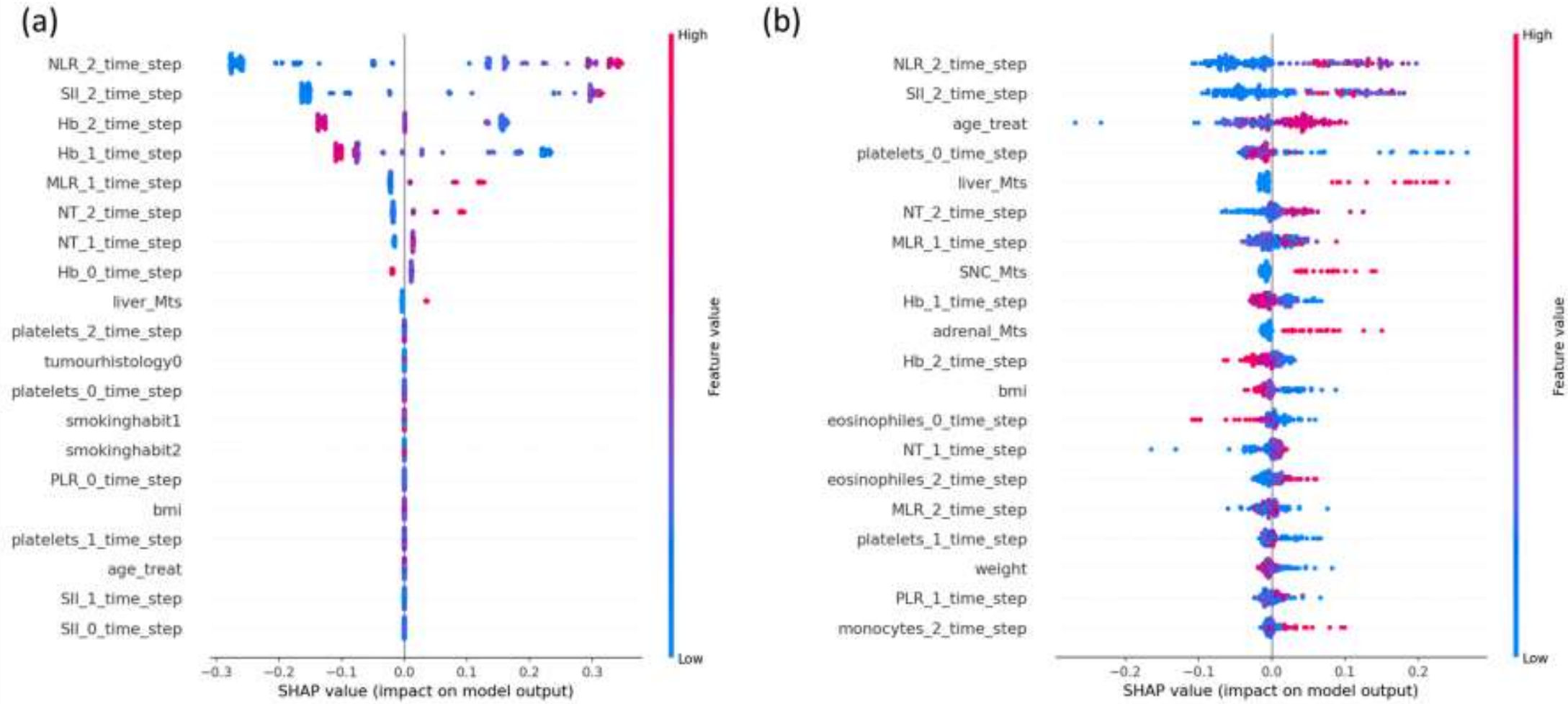

Fig. 7 Clinical model interpretation using SHAP. The summary plots show each clinical data impact on longitudinal RF model for endpoint PFS6 (**a**) and endpoint PFS9 (**b**). A positive SHAP value indicates an increased risk of progression. Each point in the summary plot represents a patient

Conclusions and future perspectives

- Diagnosis, radiomic and Deep-radiomics models will be integrated in clinical routine

  Radiomic models useful to assess malignancy and subtypes

  Future

  Efficiency improvement -> Integration in commercial systems

  Screening scheduling assisted by risk assessment

  Radiomic based tumor subtyping could enable plasma first strategies

Conclusions and future perspectives

- Immunotherapy response prediction

Multimodal and spatio-temporal models useful in predicting response to immunotherapy stage IV NSCLC

Future

Assessment of complete response or partial response in earlier stages (stage III no resectable, stages IB-IIIA adyuvant or neoadyuvant regimes)

New therapies assessment and workflow integration

Effectiveness evaluation in clinical trials

AI to better understand the mechanisms of immunotherapy and its effectiveness

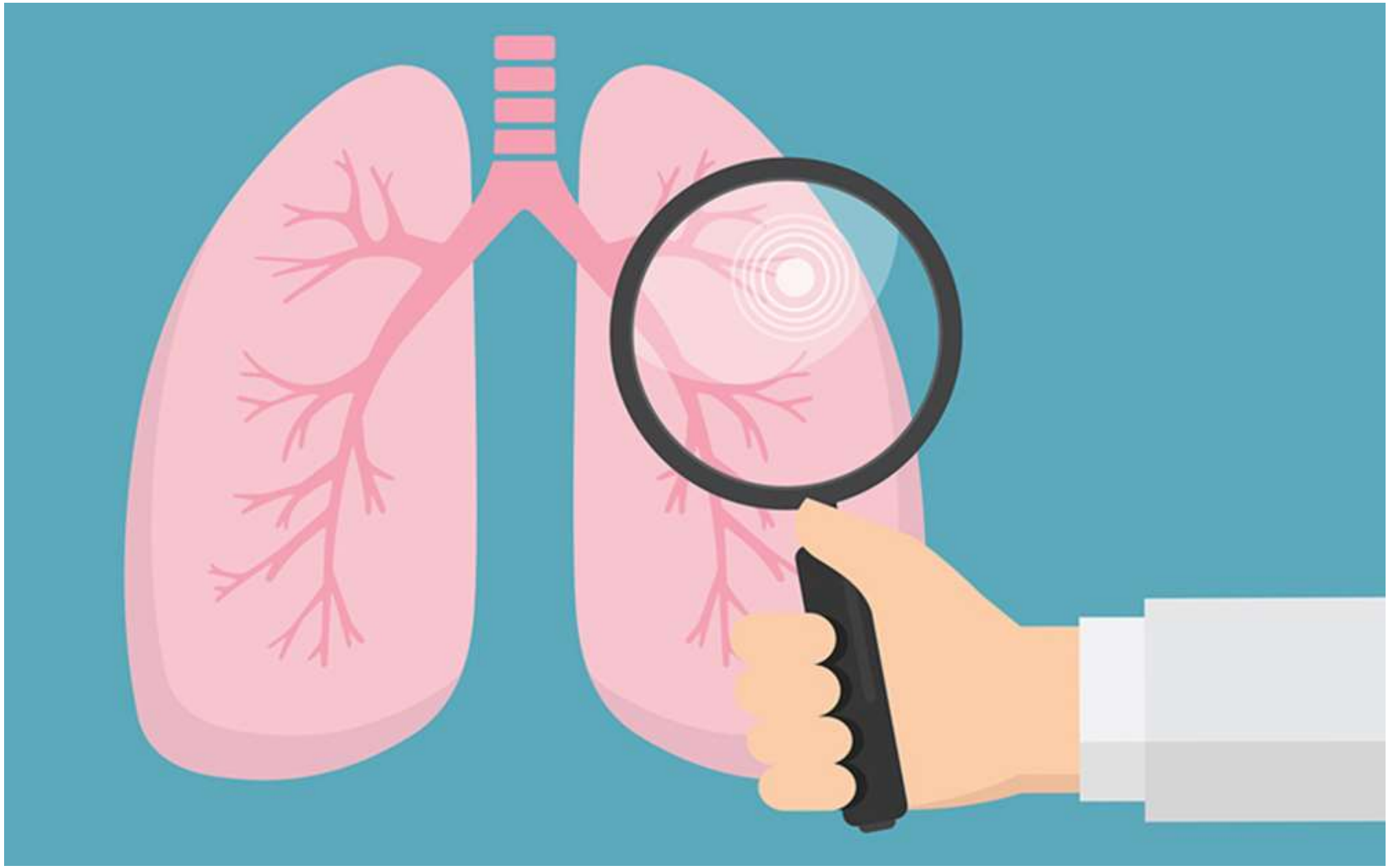

Acnowledgments

- Benito Farina
- Raul San José-Estepar
- Gonzalo Vegas Sánchez-Ferrero
- Juan Enrique Ortuño
- Ana Delia Ramos Guerra
- Luis Seijo Maceiras
- Manuel Domine Gómez
- Germán Peces-Barba
- Ignacio Gil-Bazo
- Luis Paz Arés
- Consorcio Ingenio

16th CONGRESS Lung ON CANCER

BARCELONA 27 / 28 NOVEMBER 2025

Radiomics in lung cancer applied to diagnosis and prediction

María Jesús Ledesma Carbayo

ciber | BBN

POLITÉCNICA

GECP lung cancer research

16th CONGRESS Lung ON CANCER

BARCELONA 27 / 28 NOVEMBER 2025

THANK YOU

mj.ledesma@upm.es

GECP lung cancer research

Datos clínicos y laboratorio

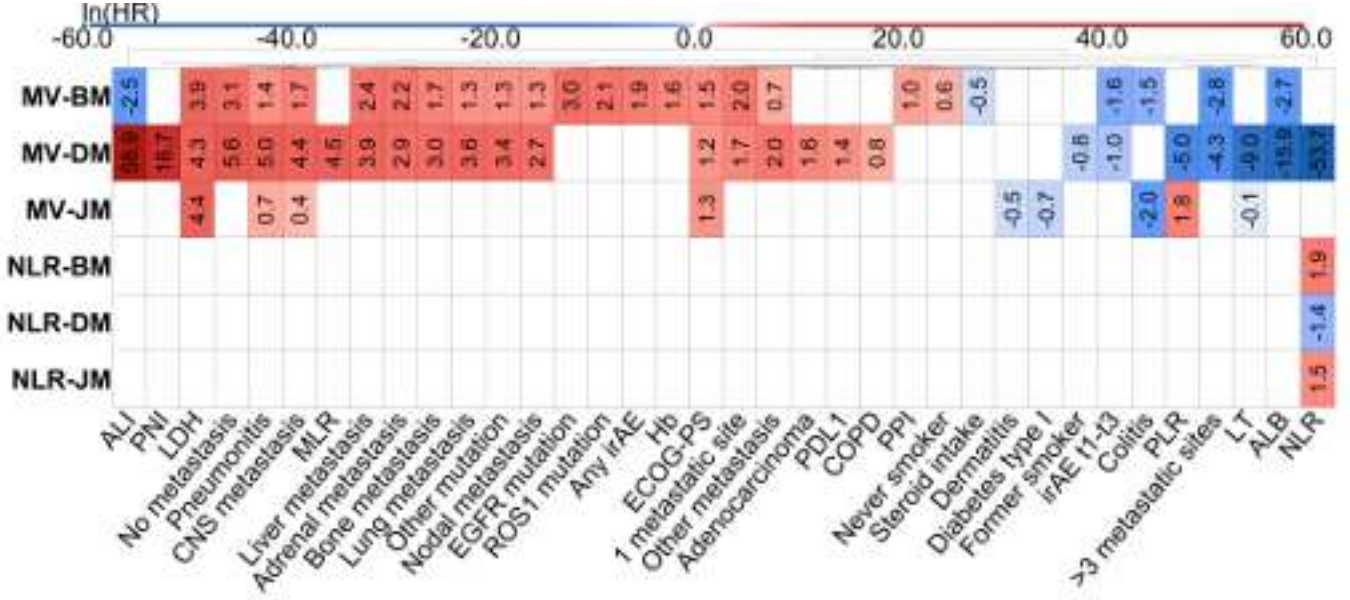

. Datos clínicos y analítica longitudinal

212 pacientes FJD - entrenamiento

137 CUN y 75 H12O cohortes independientes

. Modelos bayesianos longitudinales vs basales y delta

. NLR vs modelo multivariado MV

. Modelos longitudinales mucho mejor capacidad de respuesta

. MV-JM más sensible y específico

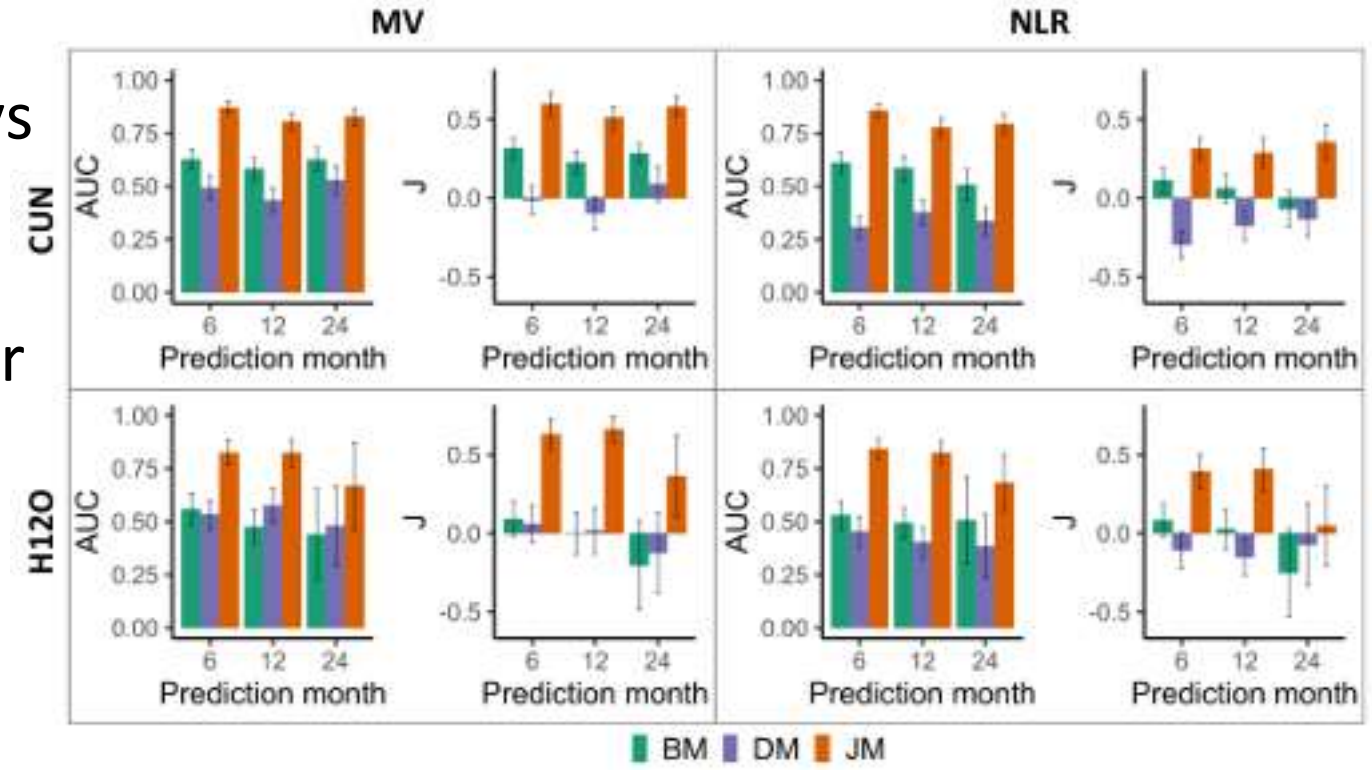

Ramos Guerra et al. 2025

Datos clínicos y laboratorio

. Datos clínicos y analítica longitudinal

212 pacientes FJD - entrenamiento

137 CUN y 75 H12O cohortes independientes

. Modelos bayesianos longitudinales vs basales y delta

. NLR vs modelo multivariado MV

. Modelos longitudinales mucho mejor capacidad de respuesta

. MV-JM más sensible y específico

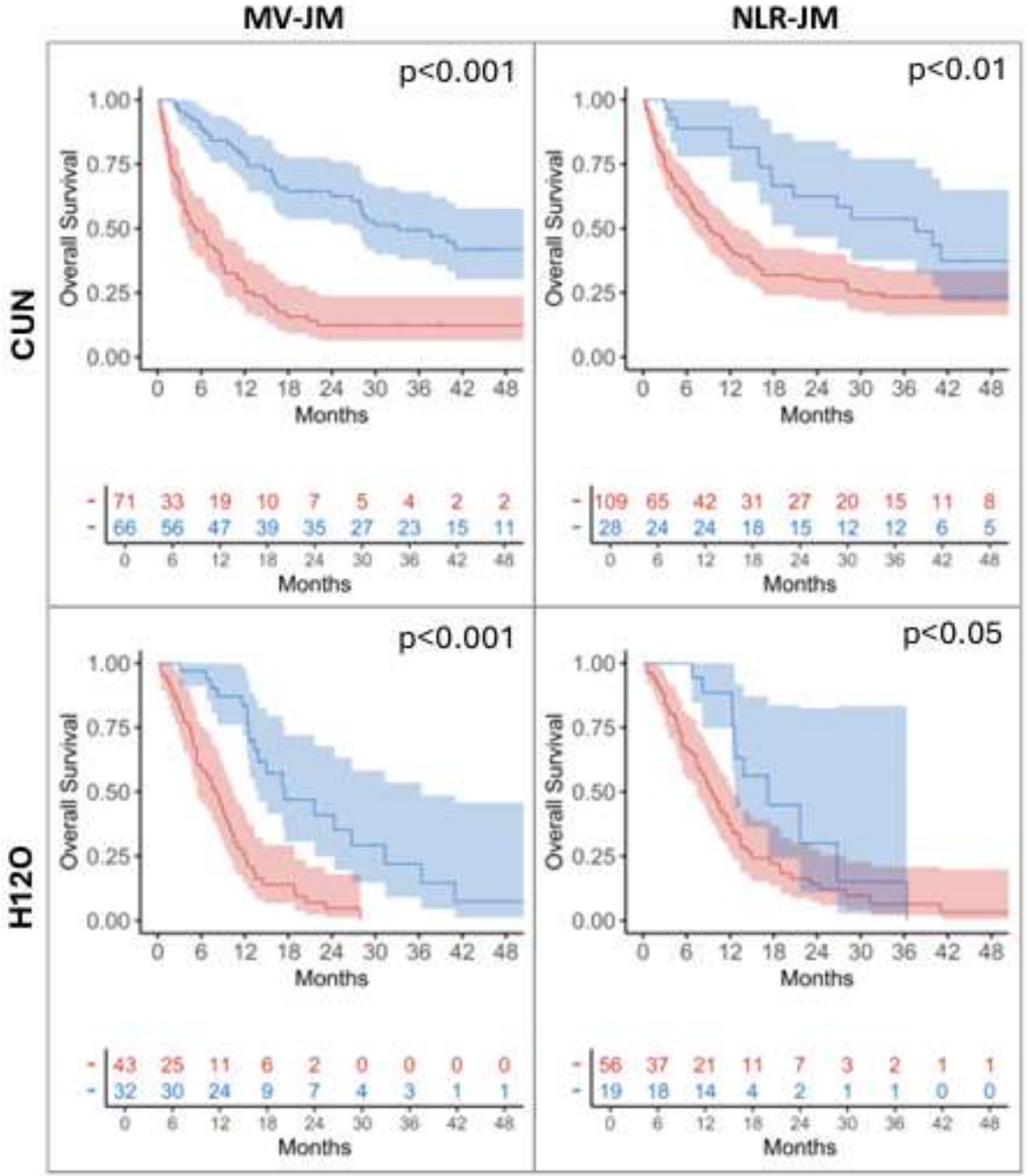

Ramos Guerra et al. Cancer Immunology Immunotherpy 2025

Predicción de respuesta a partir de inmuhohistoquimica y patología digital

Ligero M, et al (2024): **Weakly Supervised Deep Learning Predicts Immunotherapy Response in Solid Tumors Based on PD-L1 Expression**

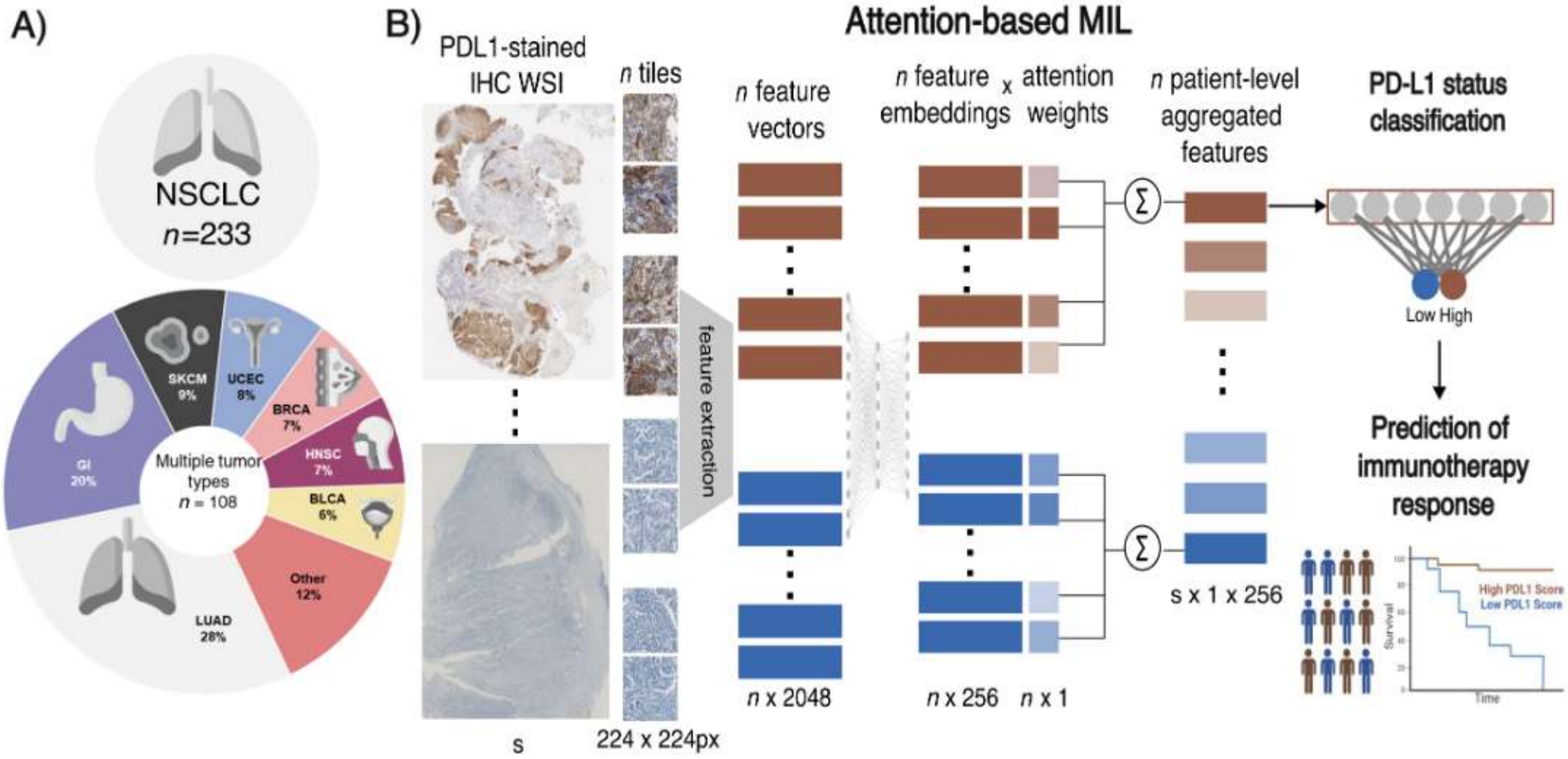

Data from 3 hospitals (1 external, 2 from INGENIO)

382 WSIs

M. Ligero et al results
Path encoder: RetCCL
N test =108. TPS <1 vs. ≥1%
AUC = 0.8

AUC Mean and SD (5 fold CV)

Patch Encoder	TPS <1% AUC	TPS 1-49 % AUC	TPS ≥50% AUC	AUC macro
CTransPath '21	0.918 ± 0.031	0.799 ± 0.034	0.948 ± 0.025	0.888 ± 0.015
RetCCL '21	0.867 ± 0.033	0.747 ± 0.090	0.928 ± 0.025	0.847 ± 0.038
HIPT$_{256}$ (TCGA) '22	0.841 ± 0.059	0.722 ± 0.076	0.927 ± 0.023	0.830 ± 0.044
PLIP '23	0.913 ± 0.036	0.813 ± 0.052	0.959 ± 0.014	0.895 ± 0.029
Phikonv2 '24	0.934 ± 0.023	0.831 ± 0.037	0.964 ± 0.014	0.910 ± 0.017
Virchow2 '24	**0.936** ± 0.011	0.844 ± 0.069	0.977 ± 0.021	**0.919** ± 0.029
Hoptimus1 '25	0.921 ± 0.024	0.844 ± 0.016	0.978 ± 0.010	0.914 ± 0.009
CONCHv1.5 '25	0.911 ± 0.029	0.847 ± 0.051	**0.979** ± 0.010	0.912 ± 0.028
UNI2-h '25	0.935 ± 0.022	**0.858** ± 0.045	0.963 ± 0.018	**0.919** ± 0.022
Pretrained HIPT$_{256}$ '25	0.932 ± 0.024	0.826 ± 0.053	0.959 ± 0.032	0.905 ± 0.020

Ramos Guerra et al. en proceso de publicación